AERO. & ASTRO. LIBRARY

MASS. INST. TECH. [redacted] ENG. LIBRARY

NOV 28 1933

To: Library, Massachusetts Institute of Technology

NATIONAL ADVISORY COMMITTEE FOR AERONAUTICS

REPORT No. 463

Copy #3

THE N.A.C.A. HIGH-SPEED WIND TUNNEL AND TESTS OF SIX PROPELLER SECTIONS

By JOHN STACK

1933

For sale by the Superintendent of Documents, Washington, D.C. - - - - - - - - - - - - - - - - Price 1 cents

AERONAUTICAL SYMBOLS

1. FUNDAMENTAL AND DERIVED UNITS

	Symbol	Metric		English	
		Unit	Symbol	Unit	Symbol
Length	l	meter	m	foot (or mile)	ft. (or mi.)
Time	t	second	s	second (or hour)	sec. (or hr.)
Force	F	weight of 1 kilogram	kg	weight of 1 pound	lb.
Power	P	kg/m/s		horsepower	hp.
Speed		km/h	k.p.h.	mi./hr	m.p.h.
		m/s	m.p.s.	ft./sec	f.p.s.

2. GENERAL SYMBOLS, ETC.

W, Weight $= mg$

g, Standard acceleration of gravity $= 9.80665$ m/s^2 $= 32.1740$ ft./sec.^{2}

m, Mass $= \frac{W}{g}$

ρ, Density (mass per unit volume).

Standard density of dry air, 0.12497 (kg-m^{-4} s^2) at 15° C. and 750 mm $= 0.002378$ (lb.-ft.$^{-4}$ sec.^{2}).

Specific weight of "standard" air, 1.2255 kg/m^3 $= 0.07651$ lb./ft.^{3}.

mk^2, Moment of inertia (indicate axis of the radius of gyration k, by proper subscript).

S, Area.

S_w, Wing area, etc.

G, Gap.

b, Span.

c, Chord.

$\frac{b^2}{S}$, Aspect ratio.

μ, Coefficient of viscosity.

3. AERODYNAMICAL SYMBOLS

V, True air speed

q, Dynamic (or impact) pressure $= \frac{1}{2}\rho V^2$.

L, Lift, absolute coefficient $C_L = \frac{L}{qS}$

D, Drag, absolute coefficient $C_D = \frac{D}{qS}$

D_o, Profile drag, absolute coefficient $C_{Do} = \frac{D_o}{qS}$

D_i, Induced drag, absolute coefficient $C_{Di} = \frac{D_i}{qS}$

D_p, Parasite drag, absolute coefficient $C_{Dp} = \frac{D_p}{qS}$

C, Cross-wind force, absolute coefficient $C_C = \frac{C}{qS}$

R, Resultant force.

i_w, Angle of setting of wings (relative to thrust line).

i_t, Angle of stabilizer setting (relative to thrust line).

Q, Resultant moment.

Ω, Resultant angular velocity.

$\rho\frac{Vl}{\mu}$, Reynolds Number, where l is a linear dimension.

e.g., for a model airfoil 3 in. chord, 100 mi./hr. normal pressure, at 15° C., the corresponding number is 234,000;

or for a model of 10 cm chord 40 m/s, the corresponding number is 274,000.

C_p, Center of pressure coefficient (ratio of distance of c. p. from leading edge to chord length).

α, Angle of attack.

ϵ, Angle of downwash.

α_o, Angle of attack, infinite aspect ratio

α_i, Angle of attack, induced.

α_a, Angle of attack, absolute.
(Measured from zero lift position.)

γ, Flight path angle.

REPORT No. 463

THE N.A.C.A. HIGH-SPEED WIND TUNNEL AND TESTS OF SIX PROPELLER SECTIONS

By JOHN STACK

Langley Memorial Aeronautical Laboratory

NATIONAL ADVISORY COMMITTEE FOR AERONAUTICS

NAVY BUILDING, WASHINGTON, D.C.

(An independent Government establishment, created by act of Congress approved March 3, 1915, for the supervision and direction of the scientific study of the problems of flight. Its membership was increased to 15 by act approved March 2, 1929 (Public, No. 908, 70th Congress). It consists of members who are appointed by the President, all of whom serve as such without compensation.)

JOSEPH S. AMES, Ph.D., *Chairman*,
President, Johns Hopkins University, Baltimore, Md.
DAVID W. TAYLOR, D.Eng., *Vice Chairman*,
Washington, D.C.
CHARLES G. ABBOT, Sc.D.,
Secretary, Smithsonian Institution, Washington, D.C.
LYMAN J. BRIGGS, Ph.D.,
Director, Bureau of Standards, Washington, D.C.
ARTHUR B. COOK, Captain, United States Navy,
Assistant Chief, Bureau of Aeronautics, Navy Department, Washington, D.C.
WILLIAM F. DURAND, Ph.D.,
Professor Emeritus of Mechanical Engineering, Stanford University, California.
BENJAMIN D. FOULOIS, Major General, United States Army,
Chief of Air Corps, War Department, Washington, D.C.
HARRY F. GUGGENHEIM, M.A.,
Port Washington, Long Island, New York.
ERNEST J. KING, Rear Admiral, United States Navy,
Chief, Bureau of Aeronautics, Navy Department, Washington, D.C.
CHARLES A. LINDBERGH, LL.D.,
New York City.
WILLIAM P. MACCRACKEN, Jr., Ph.B.,
Washington, D.C.
CHARLES F. MARVIN, Sc.D.,
Chief, United States Weather Bureau, Washington, D.C.
HENRY C. PRATT, Brigadier General, United States Army,
Chief, Matériel Division, Air Corps, Wright Field, Dayton, Ohio.
EDWARD P. WARNER, M.S.,
Editor "Aviation," New York City.
ORVILLE WRIGHT, Sc.D.,
Dayton, Ohio.

GEORGE W. LEWIS, *Director of Aeronautical Research.*
JOHN F. VICTORY, *Secretary.*
HENRY J. E. REID, *Engineer in Charge, Langley Memorial Aeronautical Laboratory, Langley Field, Va.*
JOHN J. IDE, *Technical Assistant in Europe, Paris, France.*

EXECUTIVE COMMITTEE

JOSEPH S. AMES, *Chairman.*
DAVID W. TAYLOR, *Vice Chairman.*

CHARLES G. ABBOT.
LYMAN J. BRIGGS.
ARTHUR B. COOK.
BENJAMIN D. FOULOIS.
ERNEST J. KING.
CHARLES A. LINDBERGH.
WILLIAM P. MACCRACKEN, Jr.
CHARLES F. MARVIN.
HENRY C. PRATT.
EDWARD P. WARNER.
ORVILLE WRIGHT.

JOHN F. VICTORY, *Secretary.*

REPORT No. 463

THE N.A.C.A. HIGH-SPEED WIND TUNNEL AND TESTS OF SIX PROPELLER SECTIONS

By John Stack

SUMMARY

This report gives a description of the high-speed wind tunnel of the National Advisory Committee for Aeronautics. The operation of the tunnel is also described and the method of presenting the data is given. An account of an investigation of the aerodynamic properties of six propeller sections is included.

The tunnel is operated on the induction-jet principle. Compressed air discharged through an annular nozzle surrounding the tunnel downstream from the test section induces a flow of air from the atmosphere through the test section of the tunnel where the models are placed. The forces on the model are measured by a 3-component photo-recording balance.

The test results included herein comprise measurements of the lift, drag, and pitching moments of six airfoils. The sections chosen for tests have thickness ratios of 0.06, 0.08, and 0.10; three are based on the Clark Y profile and three on the R.A.F. 6 profile. The tests were made over a wide speed range and for several angles of attack, varying from that of zero lift to 12°, in order to investigate the effects of compressibility on the airfoil characteristics.

The data obtained indicate that the Clark Y airfoils are superior to the R.A.F. 6 airfoils for propeller applications except for high-pitch propellers operating at low values of V/nD. The effects of compressibility on the airfoil characteristics are large and important. As the speed of the air flowing past an airfoil is increased the lift, drag, and moment coefficients undergo a small numerical increase which continues until a compressibility burble occurs. As the speed is increased further, the breakdown of the flow corresponding to the compressibility burble is evidenced by a marked decrease in the lift coefficient and a rapid increase in the drag coefficient. The speed at which the compressibility burble occurs is dependent on the angle of attack and the airfoil thickness; increasing either causes the compressibility burble to occur at lower speeds. A comparison of these data with the theoretical work of Glauert and Ackeret as regards the nature and amount of the effects of compressibility on the lift-curve slope substantiates the theory for speeds below that at which the compressibility burble occurs.

A computation of propeller characteristics based on these results is compared with the experimental results on a full-scale propeller. The reasons for differences are discussed and recommendations for future work are given.

INTRODUCTION

The advantages of model testing as an aid to the solution of full-scale problems are often neutralized by the inaccurate reproduction of the full-scale flow in the model test. The conditions which must be fulfilled in the model test so that the results may be directly applicable to the full-scale problem are twofold. First, the model must be geometrically similar to the full-scale object—a condition usually obtained—and second, the model flow pattern must be similar to the full-scale flow pattern—a condition generally not fulfilled. The principal factors that determine flow similarity are the Reynolds Number $\rho Vl/\mu$ and the compressibility factor V/V_c where V_c is the velocity of sound in the gas. The first of these two factors, the Reynolds Number, expresses the ratio of the mass forces to the viscous forces in the fluid. It is essential that this ratio have the same value for the model flow as for the full-scale flow. The second factor, the ratio of the velocity of the body to the velocity of sound in the gas V/V_c, indicates to what extent the flow is affected by the compressibility of the gas. For most applications the effects of variations in the value of this ratio are neglected because the velocities of the air streams in most wind tunnels are of the same order of magnitude as the velocities of most aircraft and the effect of the differences in the value of this factor between the model flow and the full-scale flow is therefore small. In addition, the speeds common to most aircraft are low with respect to the velocity of sound in air and the corresponding pressure differences are likewise small.

A knowledge of the compressibility phenomenon is essential, however, because the tip speeds of propellers now in use are commonly in the neighborhood of the velocity of sound. Further, the speeds that have been attained by racing airplanes are as high as half the velocity of sound. Even at ordinary airplane speeds the effects of compressibility should not be disregarded if accurate measurements are desired.

Some data on the effects of compressibility are already available. Experiments on propellers rotated at very high speeds have demonstrated that large detrimental effects are to be expected as the tip speed approaches the speed of sound. These experiments, although of immediate practical value, are not well suited for a study of the compressibility phenomena. Efforts to provide more suitable data have also been made. Airfoils have been tested at high speeds, but the experiments have been conducted under unfavorable circumstances. The large amount of power required to drive a stream of air at very high speeds has necessitated the use of small wind tunnels, the characteristics of which were often unknown. Furthermore, the size of the models being large in relation to the size of the wind tunnels, the test results are subject to large corrections which are in themselves problematical.

In order to provide more suitable means for studying compressibility phenomena, the National Advisory Committee for Aeronautics has constructed a comparatively large closed-throat high-speed wind tunnel. The tunnel, which was designed to utilize compressed air from the N.A.C.A. variable-density wind tunnel as a source of motive power, was the outgrowth of experiments dealing with thrust augmentors for jet propulsion (reference 1). High-velocity compressed-air jets were employed to induce a flow of the surrounding air through the augmenting devices. The results indicated that it was possible to apply the principles of the induction jet to the development of a high-speed wind tunnel. The calculations leading to the preliminary design were started in July 1927. After a series of model tests, a 12-inch diameter open-throat high-speed tunnel was constructed in April 1928. Further developments were carried out with this tunnel from which the present closed-throat tunnel was finally evolved.

The N.A.C.A. high-speed wind tunnel has several advantages over previous devices. The diameter of the tunnel is large compared to previous tunnels in which high-speed tests have been made. The flow past the model is relatively nonturbulent, since the air stream in the tunnel throat is composed entirely of air taken directly from the atmosphere. Moreover, the models extend through the walls and are supported outside the air stream, thus eliminating the effects of support interference. Several airfoils have been tested in this tunnel and this report presents a description of the tunnel, together with the results of tests on six airfoils having commonly used propeller sections. The data presented comprise the results of tests made over a wide speed range and these data have been analyzed with a view toward demonstrating the compressibility effects and their relation to design problems.

I. DESCRIPTION OF TUNNEL

The high-speed wind tunnel is similar in form to most venturi-type wind tunnels. There are, however, important differences in its characteristics and equipment, which arise in part from its purpose and in part from the method of operation. The novel features are the large speed range which extends up to the velocity of sound when there is no model in the tunnel, the drive system, and the automatic-recording balance used to measure the forces.

Arrangement.—The general arrangement of the tunnel is shown in figures 1 and 2. Compressed air from the variable-density wind tunnel is piped to the high-pressure chamber and discharged through the annular nozzle shown in figure 2. The jet from this nozzle induces a flow of air from the atmosphere through the lower portion of the tunnel, where the model is placed on a photorecording balance as shown in figure 2. The atmospheric air mixes with the high-pressure air in the diffuser which conducts the air outside through the roof of the building.

The balance and the lower portion of the tunnel are enclosed in an airtight wooden chamber which is supported by a metal framework fastened to the floor of the building as shown in figure 1. Access to the tunnel and balance is obtained by removing two opposite sides of the chamber. One half of the test section is also removable in order to facilitate mounting the model.

Tunnel air passages.—The entrance cone is 17.67 inches long and 11 inches in diameter at its junction with the test section. Six vanes, which extend from the floor to the plane of the mouth of the entrance cone, are provided to prevent twisting of the air stream at the entrance cone. The test section is 7 inches long, and is made slightly divergent to reduce the axial static-pressure gradient. The included angle between the walls of the exit cone is 4.6°; the portion tapered at this angle is 13 5/16 inches and ends in an abrupt step just below the annular nozzle. The diffuser is 19 feet 10 inches long and the included angle between diametrically opposite elements is 4.8°.

Power supply.—The motive power for the air stream is provided by compressed air from the variable-density wind tunnel. At the end of a test at high values of the Reynolds Number in this tunnel a relatively large supply of air at high pressure is available. The compressed air is piped to the chamber surrounding the annular nozzle shown in figure 2 and discharged through the nozzle. The high-pressure chamber and the nozzle are of cast steel. The nozzle has a minimum annular opening of 0.06 inch and a divergent portion 1 5/16 inches long. The total angle of divergence is 11.1°.

TUNNEL CHARACTERISTICS

Velocity and pressure distribution.—Figure 3 indicates the dynamic-pressure variation across the tunnel along the quarter-chord position of the model. The variation is less than ±0.5 percent. The directional variation of the air flow is believed to be less than ±¼°. Figure 4 shows the small static-pressure gradient.

Energy ratio.—The energy ratio is difficult to determine for this type of tunnel because of the uncertainty of the value of the power input. For comparative purposes, however, the power input is taken as the rate of work due to an adiabatic expansion of the high-pressure air from the pressure in the reservoir to atmospheric pressure. The energy ratio is therefore defined as the quotient of the kinetic energy of the air passing through the test section in a unit time divided by the power due to adiabatic expansion of the high-pressure air. The value for the tunnel as operated varies considerably over the speed range but at a speed 0.5 V_c the value is 1.6.

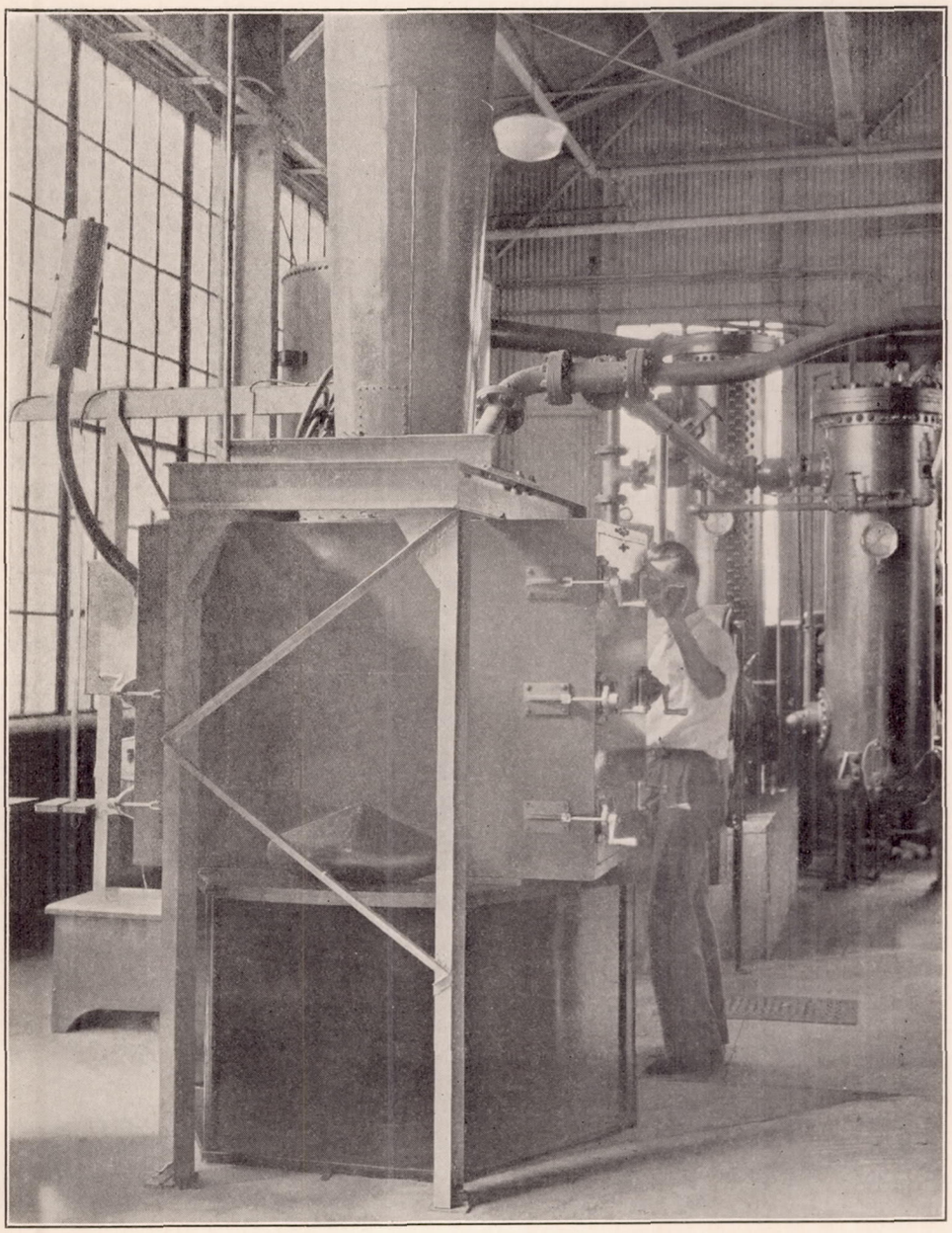

FIGURE 1.—General view of the high-speed wind tunnel.

DESCRIPTION OF THE BALANCE

General.—The balance must measure the large range of forces resulting from the wide speed range over which tests are made, and it must be automatic recording because the allowable time for observations is short. The balance measures the lift, drag, and pitching moment by multiplying and recording the deflection of steel springs (cantilever beam type) to which the forces are transmitted. The essential parts

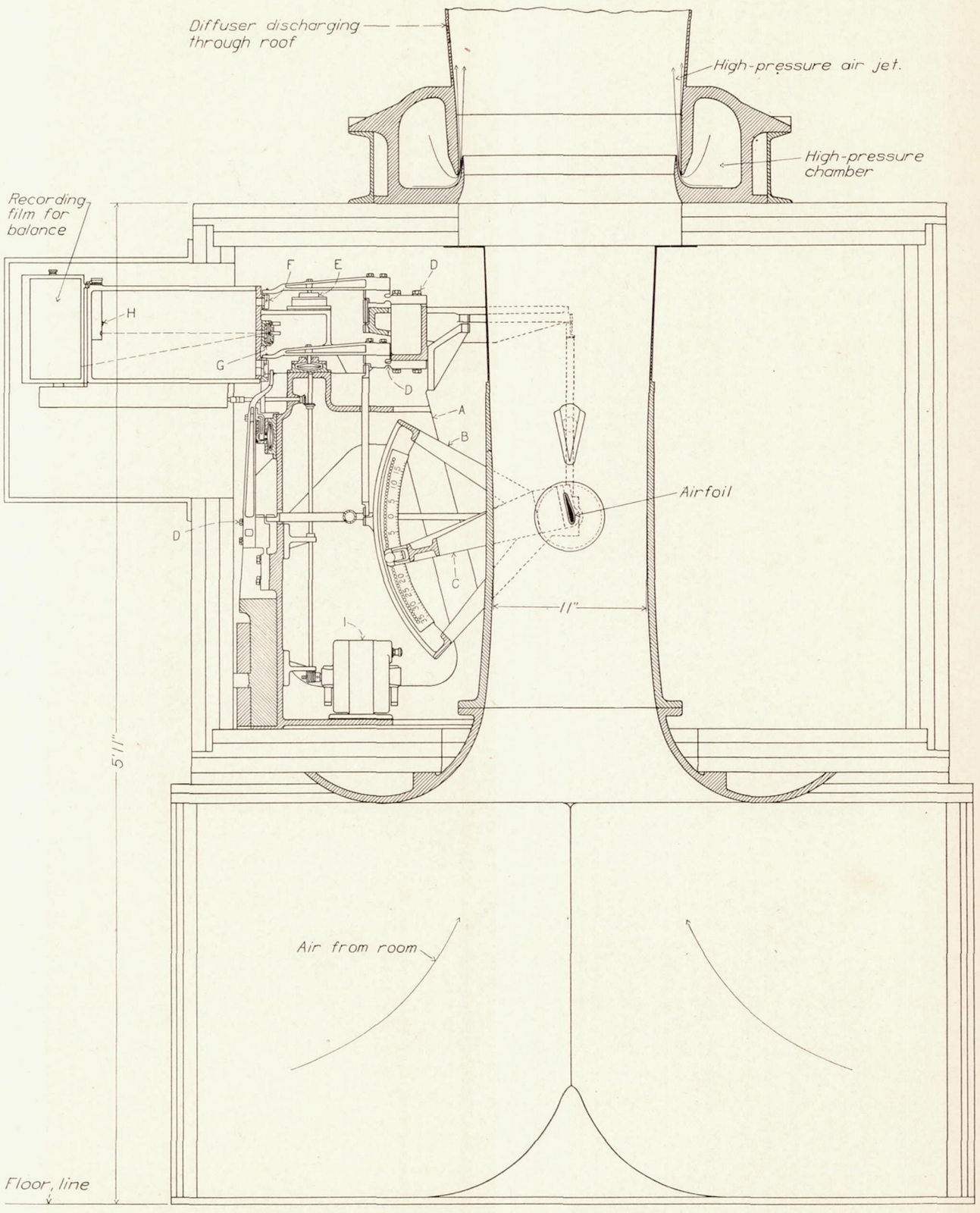

FIGURE 2.—Diagrammatic section of the high-speed wind tunnel.

A, balance frame
B, cradle
C, rotatable yoke for changing angle of attack
D, springs
E, dashpot
F, lens and mirror container
G, N.A.C.A. pressure cell
H, source light
I, film drive motor

consist of a cast-iron cradle in which is mounted a yoke to which the model is attached, the linkages necessary to transmit the forces to the steel springs, and a camera for multiplying and recording the deflections of the springs.

Linkages and knife-edges.—The balance is shown in figures 2 and 5. The cradle extends around one half of the tunnel and contains a rotatable yoke to which the model is secured. The cradle supports consist of three vertical rods, one of which is directly connected to one of the balance springs. The other two rods are connected to ends of a fork-shaped lever above the cradle. The lever is supported at its center and the other end is connected to another of the balance springs. Horizontal movement is constrained by two

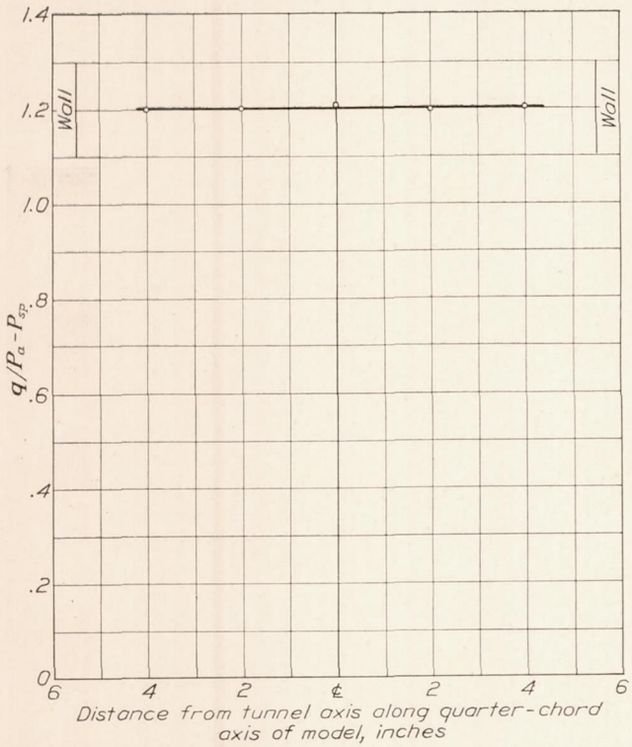

FIGURE 3.—Ratio of dynamic pressure at the test section to the difference between the atmospheric pressure and the pressure at the static-pressure orifices for velocity equal to 0.8 V_c.

rods, one on either side of the cradle, which are connected through a truss to the third balance spring.

The lift linkage transmits the horizontal or lift forces from the balance cradle to the spring at the rear of the balance. The drag and moment linkages are interacting. The drag is the algebraic sum of the forces in the three vertical supports. The forward supports are parallel to the tunnel axis and their axes are in a vertical plane which passes through the axis of the tunnel and the quarter-chord line of the models. The forces in these supports are transmitted through a fork, which is mounted on the balance frame above the cradle, to the deflecting spring shown at the top of the diagram (fig. 2). Therefore, if moments are taken about the line joining the intersection of the horizontal and vertical linkages on either side of the tunnel, the forces in these linkages will not contribute to the moment. The force in the rear support, which is connected to another deflecting spring, gives the moment directly.

Instead of the usual knife-edges, the balance linkages are connected by means of Emery knife-edges which are actually thin steel deflecting strips joining the members (figs. 2 and 5).

Springs.—All three balance springs are of the same general form, varying principally in their size, which is determined by the magnitude of the forces to be measured. They are cantilever beams of rectangular cross section, constructed of heat-treated steel, and have a short length of reduced thickness to localize the deflections. They are mounted on heavily reinforced pedestals on the rigid balance frame and are held in place by dowels and screws. The thickness of the springs is such that the deflections corresponding to the largest forces encountered are of the order of 0.005 inch.

Recording system.—Owing to the small deflections of the balance springs, the recording system must provide a large multiplication. A further requirement

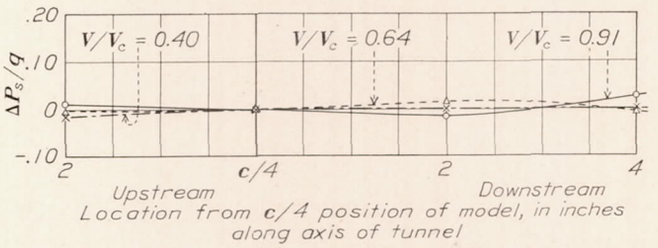

FIGURE 4.—Ratio of the change in the absolute static pressure from that at the model position to the dynamic pressure.

is the provision for sensitivity control; that is, some easy means of increasing the multiplication so that good accuracy may be maintained when the forces are comparatively small, such as those encountered at very low speeds and low angles of attack. In addition, it is necessary to record the forces automatically because of the short time during which observations must be made.

The general arrangement of the recording system is shown in figures 2 and 5. Long arms are fastened to the balance springs. At the ends of these arms a bushing is mounted in which a stylus is eccentrically fitted. By rotation of the bushing the multiplication of the beam movement can be altered. The stylus is in contact with a pivoted mirror which is thus actuated by the movement of the balance springs. Suitable damping is provided by means of dashpots connected to the spring arms. A source of light and suitable lenses are provided so that light is reflected by the mirrors to a moving film. The film is driven by a small electric motor through a train of gears which permits three speed variations. The source light and the film drive are controlled from the exterior of the balance and tunnel chamber.

Model support.—The model is mounted in jaws at the ends of the yoke. It is located by means of dowels so that the line joining the intersections of the horizontal and vertical linkages coincides with the quarter-chord axis of the model. The angle of attack is changed by rotating the yoke, which is arranged to turn about an axis through the intersection of the horizontal and vertical linkages. The yoke is fixed at various angles by means of a pin which projects from the yoke into holes in the graduated quadrant shown in figure 2.

The model extends across the tunnel and through holes in the tunnel wall. In order to reduce the flow into the tunnel from the dead-air space and to reduce interference with the air flow, these holes are covered with specially designed end plates shown in figure 6. The end plates are made of thin brass and are circular in form. They fit into recesses cut in the tunnel wall

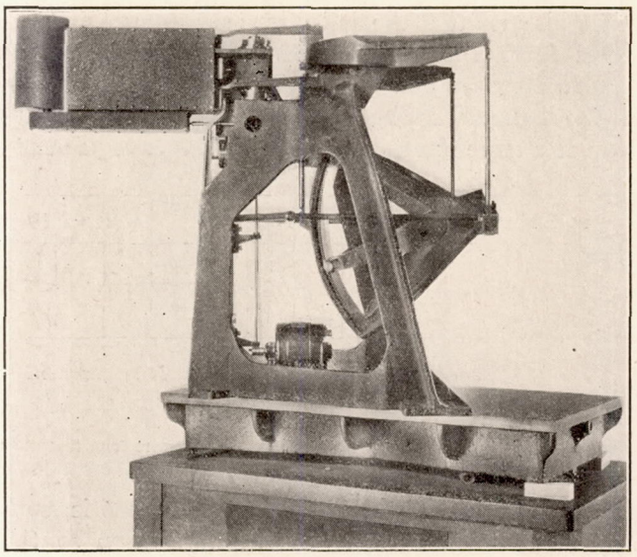

FIGURE 5.—The high-speed wind tunnel balance.

around the edges of the holes and are sufficiently flexible so that they can bend as the angle of attack is changed and thus maintain the contour of the walls. Holes of the same shape as the airfoil section but slightly larger are cut in the end plates to provide 1/16-inch clearance so that the model and the end plates cannot touch. The end plates are held in position by six U-shaped pieces. One side of each piece is soldered to the end plate and the other side carries a screw which is turned down against a ledge on the outside wall of the tunnel as shown in figure 6. The end plates can be turned with the model as the angle of attack is changed by loosening the screws in the U-shaped pieces. A telltale lamp is provided which lights if the model makes contact with the end plates during a test.

TUNNEL CALIBRATIONS

Dynamic pressure and velocity determination.—The dynamic pressure and velocity are computed from Bernouilli's equation for a compressible fluid. The equation is

$$P_a = P_s\left[1+\frac{k-1}{2}\left(\frac{V_s}{V_c}\right)^2\right]^{\frac{k}{k-1}}$$

where the subscript a denotes atmospheric conditions, the subscript s denotes conditions at the test section of the tunnel, P denotes the pressure in the fluid, V_c is the velocity of sound in the fluid for the conditions at the test section, and k is the ratio of the specific heats for air, numerically equal to 1.4. The formula is derived by substituting the pressure-density relation for adiabatic flow in the general form of the Bernouilli equation. A detailed derivation of this formula is given in reference 2 (p. 15). A more convenient form

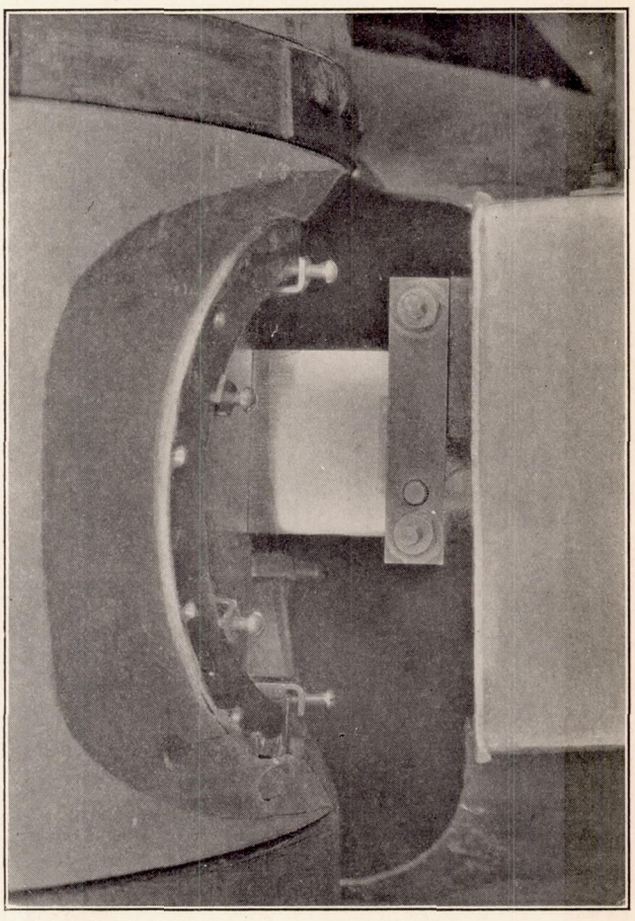

FIGURE 6.—View showing tunnel-wall fitting and airfoil mounting.

of the foregoing equation for use when V_s/V_c is less than unity is obtained by expanding in the series

$$P_a = P_s+\frac{1}{2}\rho_s V_s^2\left[1+\frac{1}{4}\left(\frac{V_s}{V_c}\right)^2+\frac{1}{40}\left(\frac{V_s}{V_c}\right)^4+\frac{1}{1600}\left(\frac{V_s}{V_c}\right)^6\cdots\right]$$

This is the form used to compute the dynamic pressure, which is therefore

$$q=\frac{1}{2}\rho_s V_s^2=\frac{P_a-P_s}{1+\frac{1}{4}\left(\frac{V_s}{V_c}\right)^2+\frac{1}{40}\left(\frac{V_s}{V_c}\right)^4+\frac{1}{1600}\left(\frac{V_s}{V_c}\right)^6\cdots}$$

The values of V_s/V_c are computed from the first form

of the equation. Solving this equation for V_s/V_c gives

$$\frac{V_s}{V_c}=\sqrt{\frac{2}{k-1}\left[\left(\frac{P_a}{P_s}\right)^{\frac{k-1}{k}}-1\right]}$$

The validity of these formulas is dependent primarily upon the existence of true adiabatic flow and the absence of losses due to friction. The errors induced by the first of these assumptions are probably small because of the rapidity with which the heat energy of the air is converted to kinetic energy. In order to check the validity of the formulas, the total pressure at the test section has been measured and it was found that its value differed from the atmospheric pressure by less than 0.02 percent of the dynamic pressure, except for a very small core at the center and a relatively thin layer adjacent to the wall.

The difference between the static pressure at the test section and the atmospheric pressure cannot be reliably determined from a direct measurement during a test because of the presence of the model. Accordingly, calibrated static-pressure orifices are used for this purpose. Four small holes in the tunnel wall 10 inches below the location of the quarter-chord axis of the model are connected to a manifold which is in turn connected to pressure-measuring devices. The calibration factor is determined from simultaneous measurements of the quantities (P_a-P_s) and (P_a-P_{sp}), where the subscript sp denotes conditions at the static-pressure orifices. The static pressure at the test section is taken as the value registered by four holes in a tube located along the axis of the tunnel. The holes in the tube are 90° apart and are in the horizontal plane which passes through the quarter-chord position of the airfoil model. In order to avoid end interferences the tube extends from the relatively low velocity region at the mouth of the entrance cone to a point 20¼ inches above the model location. The calibration factor as computed from these measurements is

$$F=\frac{q}{P_a-P_{sp}}$$

For use in computing test results both this factor and V/V_c are plotted against P_a-P_{sp}. The variation of these quantities with atmospheric pressure for constant values of P_a-P_{sp} is negligible except at speeds in the immediate neighborhood of the velocity of sound.

The only pressure measured during a test is the difference between the atmospheric pressure and the pressure at the static-pressure orifices. Two pressure-measuring devices are connected to the orifices. A single-tube mercury manometer is mounted outside the tunnel to provide the operator with means for adjusting the speed and measuring the pressure difference; a standard N.A.C.A. pressure cell (reference 3) mounted on the camera records the pressure difference on the film on which the forces are registered. The pressure cell serves to check the values observed by the operator and, in addition, gives a record of the air-flow steadiness while the observations are being taken.

Balance alinement and calibration.—The alinement of the balance linkages with respect to each other is fixed by the construction of the balance. Alinement of the balance with respect to the air-flow direction is obtained by applying an external force in the horizontal or lift direction and adjusting the height of the rear base of the balance until the drag balance indicates zero force. The air-flow alinement has been checked by testing an airfoil in the normal and inverted positions

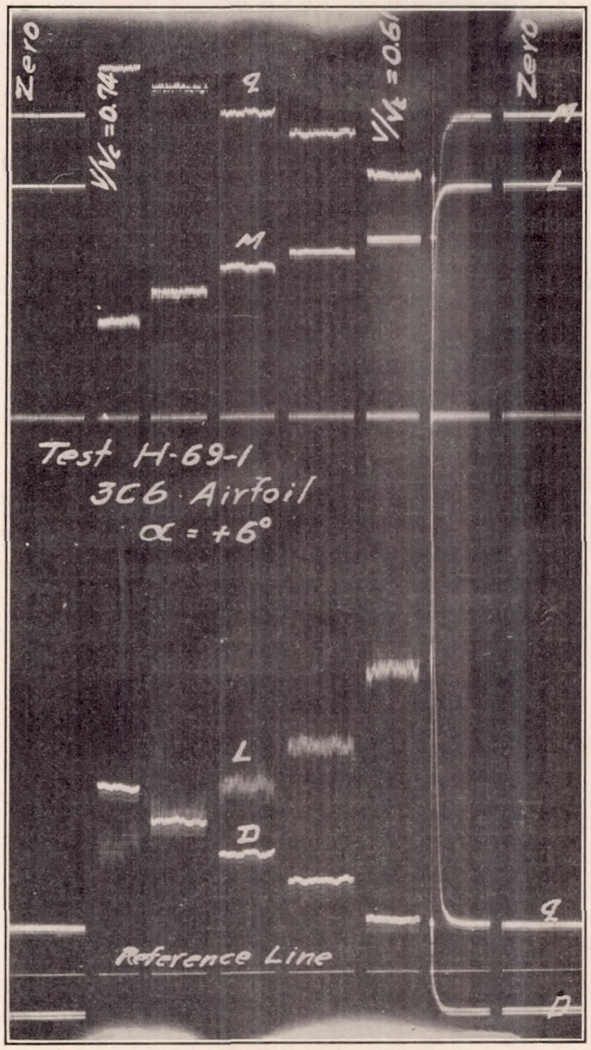

FIGURE 7.—Section of photographic record taken from balance.

and also by tests of a symmetrical airfoil at positive and negative angles of attack.

The balance calibration is obtained by applying known loads in the direction of the various forces by means of a specially designed system of levers. The deflections corresponding to these loads are recorded on the film and from these data calibration charts are constructed. Errors due to misalinement of the various levers which comprise the calibrating fixture are less than 1 part in 3,000 and the errors in the weights used in calibrating are of the order of 1 part in 700.

A TYPICAL AIRFOIL TEST

The standard airfoils, 2-inch chord, are made of metal, usually steel. They are constructed by a generating machine which works from a sixfold templet. The method of construction is described in reference 4. The extremities of the airfoil are machined flat and drilled from a jig to insure accurate mounting on the balance.

The airfoil is mounted in the balance and the angle of attack is set by means of the pivoted yoke. The chamber doors are then clamped in place. The valve in the high-pressure air duct is opened wide and when conditions become steady, as indicated by the mercury manometer, observations are taken. Lower speeds are obtained by throttling. The run is continued, with interruptions for recording zeros, until the entire speed range is covered. The chamber is then opened and the angle of attack is changed and the procedure as outlined above is repeated. The number of angles of attack for which tests can be obtained from one tank of air is dependent on the number of speeds for which observations are made. Even when a relatively large number of observations for various speeds are taken, complete observations for two angles of attack can be made. The tunnel operating time required for testing an airfoil at one angle of attack over the entire speed range is approximately 12 minutes.

The forces and moments are evaluated from the photographic record (fig. 7). The deflections indicated on the film are measured by means of a special device and the forces corresponding to these deflections are read from the calibration charts. The data are then reduced to the standard nondimensional coefficient form.

PRESENTATION OF DATA

The effect of the tunnel walls on the aerodynamic characteristics of airfoils tested in this tunnel is not definitely known or understood. The effect of variations in the form and clearance of the end plates is known to be critical and, accordingly, the end plates are very carefully adjusted. Some preliminary tests with airfoils having different chords indicate that no correction need be applied to these data to obtain characteristics for infinite aspect ratio. In other words, it is believed that the data may be directly applied in practical design problems as airfoil data for infinite aspect ratio.

The data are presented in two graphic forms. The first form, which shows directly the effects of compressibility, consists of plots of the various coefficients for a given angle of attack against V/V_c. The other form consists of plots of the lift coefficient and the drag coefficient against angle of attack for several speeds.

II. TESTS OF SIX COMMONLY USED PROPELLER AIRFOILS AT HIGH SPEEDS

The prediction of propeller performance is dependent to a large extent on an accurate determination of the aerodynamic characteristics of the airfoil sections which are used as the propeller blade sections. Heretofore, it has been common practice to adopt the results of airfoil tests at low speeds in conventional wind tunnels for this purpose. The effects of compressibility have usually been neglected, because of the lack of the information necessary to establish a valid correction for this effect. The first series of tests in the high-speed wind tunnel was performed to provide more accurate data on which the design of propellers could be based.

TESTS

Models.—Of the 6 airfoils tested, 3 have sections based on the R.A.F. 6 section and 3 on the Clark Y section. In each group of three, the airfoil thickness is the major variable. The thickness ratios chosen are 0.06, 0.08, and 0.10, and the airfoil profiles were obtained by scaling the ordinates of the original airfoil, measured from the chord line, in the ratio of the desired thickness to the thickness of the basic section. The ordinates are given in table I. The airfoils are designated as in reference 5 by a system of numbers and a letter. Thus, the designation 3C6 is applied to the 6 percent thick Clark Y airfoil. The first number gives the location of the maximum thickness in tenths of the chord, the letter indicates the basic section from which the airfoil is derived, C for the Clark Y and R for the R.A.F. 6, and the last numbers give the maximum thickness of the airfoil in percent of the chord. The six airfoils are then the 3C6, 3C8, 3C10, 3R6, 3R8, and 3R10.

All of the airfoils were of 2-inch chord. Four were made of duralumin. The two thinnest airfoils, however, were made of steel in order to reduce the deflections of the models under high lift loads. A detailed description of the method of constructing the airfoils is given in reference 4.

Method of testing.—Because of the large range of forces involved in testing the airfoils over a wide angle-of-attack range and a wide speed range, the tests were performed in two parts. The lift and drag balances were set for maximum sensitivity and the airfoils were tested at low angles of attack; that is, up to 4°. Then, in order to permit recording the larger forces for the higher angles of attack, the sensitivities of the lift and drag balances were reduced and the high angle-of-attack tests were performed. Because of the small clearance between the airfoil and the hole in the end plates through which the airfoil protrudes, additional end plates were required for the high angle-

of-attack tests. The holes in the end plates were kept the same size as formerly but were moved slightly to one side to prevent the airfoil from touching and to keep the clearance as uniform as possible throughout the tests as the airfoil deflected under the high loads encountered at high angles of attack.

The tests in each part were made in pairs, airfoils of the same thickness being tested consecutively. The operating procedure was identical in other respects with the description previously given.

PRECISION

The various factors contributing to inaccuracy in these experiments may, in general, be classified under two major divisions. The first consists of errors in measurements made to determine the dynamic pressure and the second consists of errors in the evaluation of the actual forces and moments.

Inaccuracies arising from the dynamic-pressure variation across the throat are insignificant. The value of the static-plate calibration factor was checked over the speed range three times while the tests were in progress. The maximum differences found were approximately 1 percent. Determinations of this factor may, however, have a consistent error due to a constriction effect at the throat when the airfoil is in position. The magnitude of this error is unknown, and because of the difficult nature of the problem, a satisfactory solution has not yet been obtained. Accordingly, no correction has been applied.

Balance calibrations before and after each group of tests agreed very closely. The lift calibrations agreed to within 1.5 percent and the drag calibrations agreed to within 1 percent. The differences in the moment calibrations were less than either of the above and may be considered negligible. The evaluation of tare corrections resulting from air leakage where the model passes through the tunnel wall was not feasible. However, tests made with no model in place and with the holes in the tunnel wall closed indicated the presence of small tare readings of uncertain origin for which the data have been corrected. The magnitudes of these corrections are -0.020 for the lift coefficient, 0.0005 for the drag coefficient, and 0.020 for the moment coefficient. These corrections have been checked by repeat tests to within 0.001 for the lift, 0.0003 for the drag, and 0.005 for the moment. A few repeat tests of those airfoils at various angles of attack indicated that the results could be reproduced to within 3 percent except for high angles of attack at high speeds, when the flow was unsteady.

RESULTS

The results of the tests are presented in figures 8 to 13, inclusive. These figures show the variation in the force and moment coefficients with speed for a given angle of attack. Complete data for one airfoil are presented in each figure, each curve showing the variation of one of the three coefficients over the speed range for one angle of attack. In the presentation of the moment-coefficient data, the origin of the axes for each angle of attack has been raised above that for the previous angle of attack so that the moment curve for any angle may be easily distinguished.

Additional figures are presented to show the aerodynamic characteristics of the airfoils in more familiar form and also to illustrate further the effects of compressibility on the important characteristics. Figures 14 to 19, inclusive, are plots of the lift and drag coefficients against angle of attack. These curves are presented for several speeds to provide an easy comparison with previous work. Figure 20 shows the variation of the drag coefficients of all six airfoils with speed for three values of the lift coefficient and, in addition, the variation of the minimum drag with speed is shown. Figure 21 illustrates the effect of compressibility on the slope of the lift curve. Figures 22 and 23 illustrate an application of these data to the computation of propeller characteristics.

DISCUSSION

Comparison of airfoils.—The comparison of these airfoils should be made on the basis of lowest profile-drag coefficient for any fixed value of the lift coefficient because this characteristic is generally of paramount importance in the selection of airfoil sections for propellers. If airfoils of like thickness are compared, it is apparent from figure 20 that the C airfoils have lower profile-drag coefficients than the corresponding R airfoils except at high values of the lift coefficient. However, the differences at high values of the lift coefficient are slight except for the thinnest sections at low speeds. The reason for the advantage of the 3R6 airfoil over the 3C6 airfoil is apparent from an examination of figures 14 and 17. The maximum lift coefficient of the 3C6 airfoil is lower than that for the 3R6 airfoil and the consequent earlier burble of the C airfoil causes its efficiency to drop sooner than the efficiency for the corresponding R airfoil. Further examination of figures 14 to 19 indicates that all the C airfoils burble at somewhat lower lift coefficients than the corresponding R airfoils.

It is apparent from this comparison that C airfoils are, in general, superior to corresponding R sections for propeller applications except for very high-pitch propellers operating at low values of V/nD where the angles of attack of the propeller blade sections are in the region of maximum lift. This conclusion is in substantial agreement with previous propeller tests (reference 6).

The differences between the moment coefficients for corresponding airfoils of the two families are relatively unimportant for propeller application, but it is to be noted that the differences over the entire speed range are in accord with the results of previous low-speed tests. The lift-curve slopes (taken as the slope of the

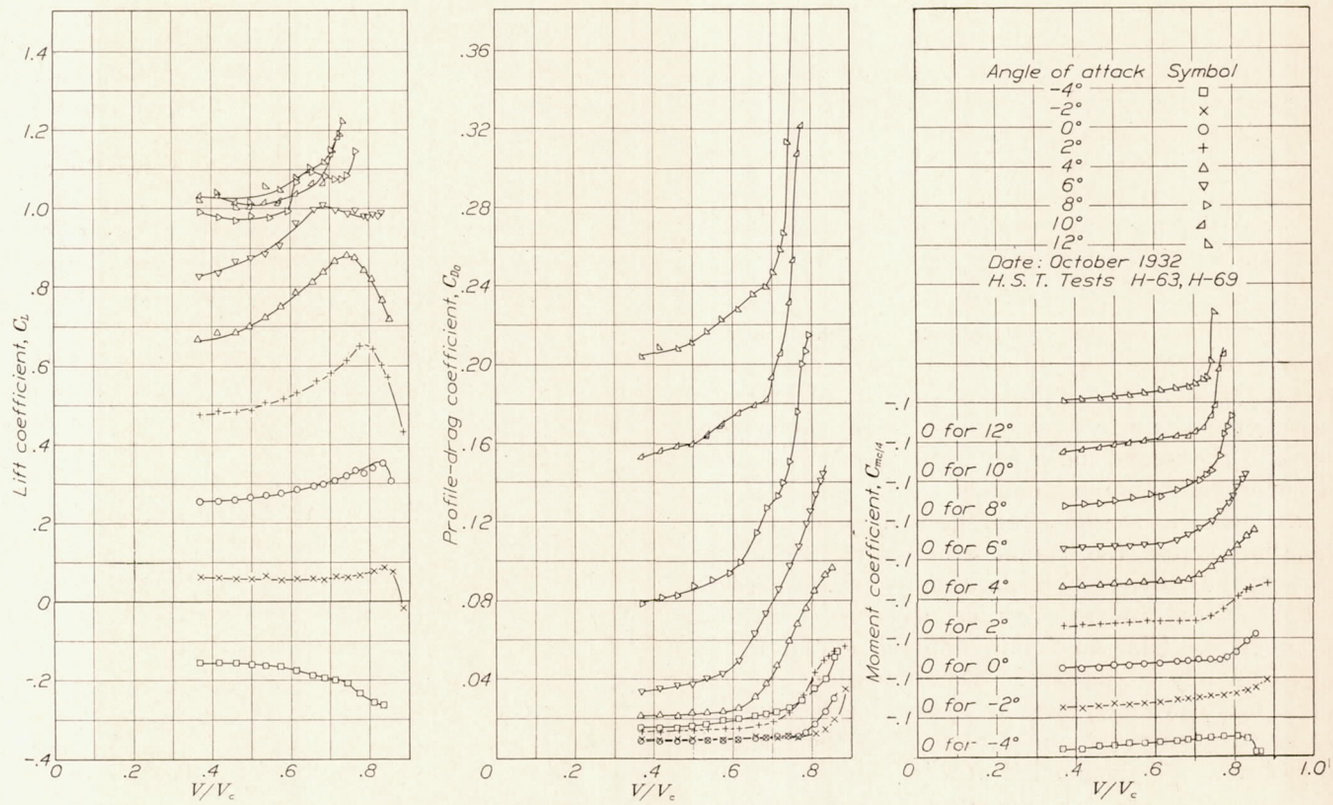

FIGURE 8.—Effects of compressibility on the aerodynamic characteristics of the 3C6 airfoil.

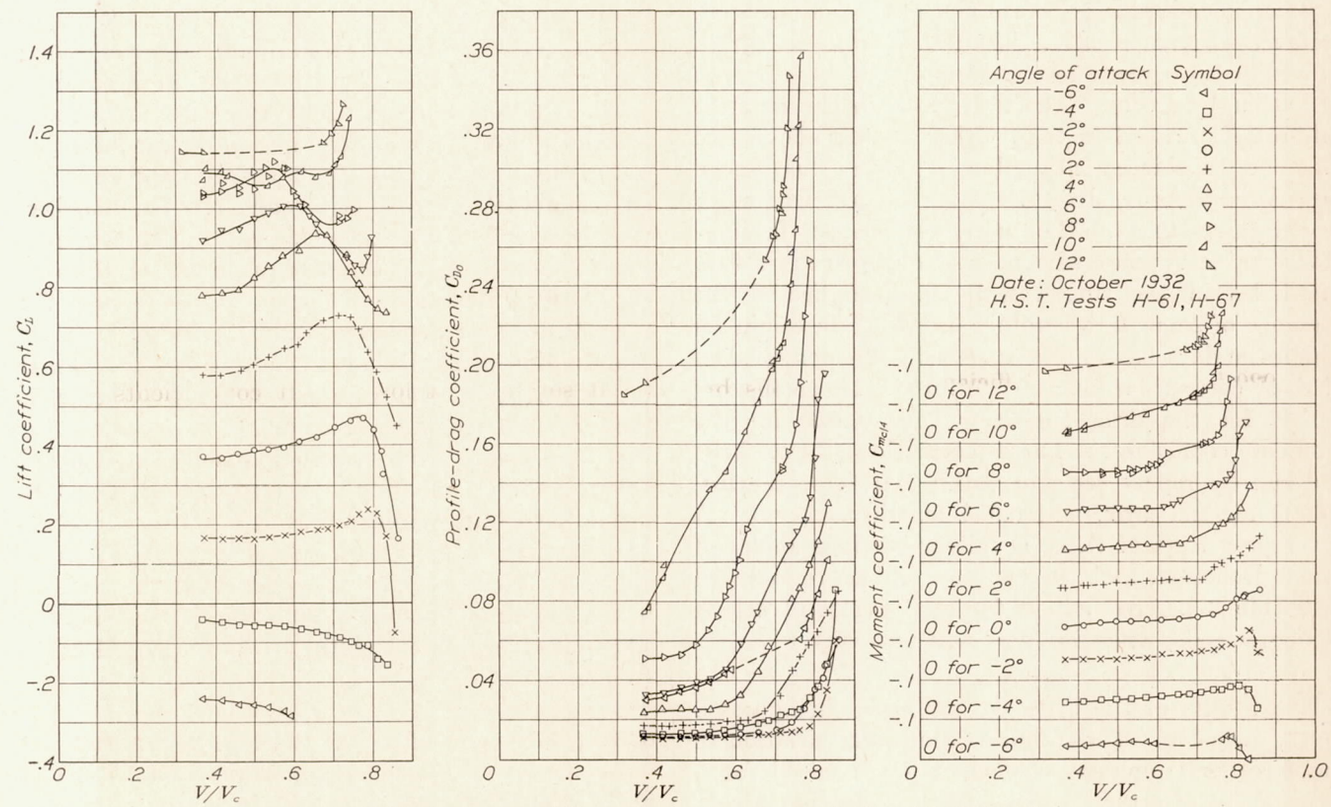

FIGURE 9.—Effects of compressibility on the aerodynamic characteristics of the 3C8 airfoil.

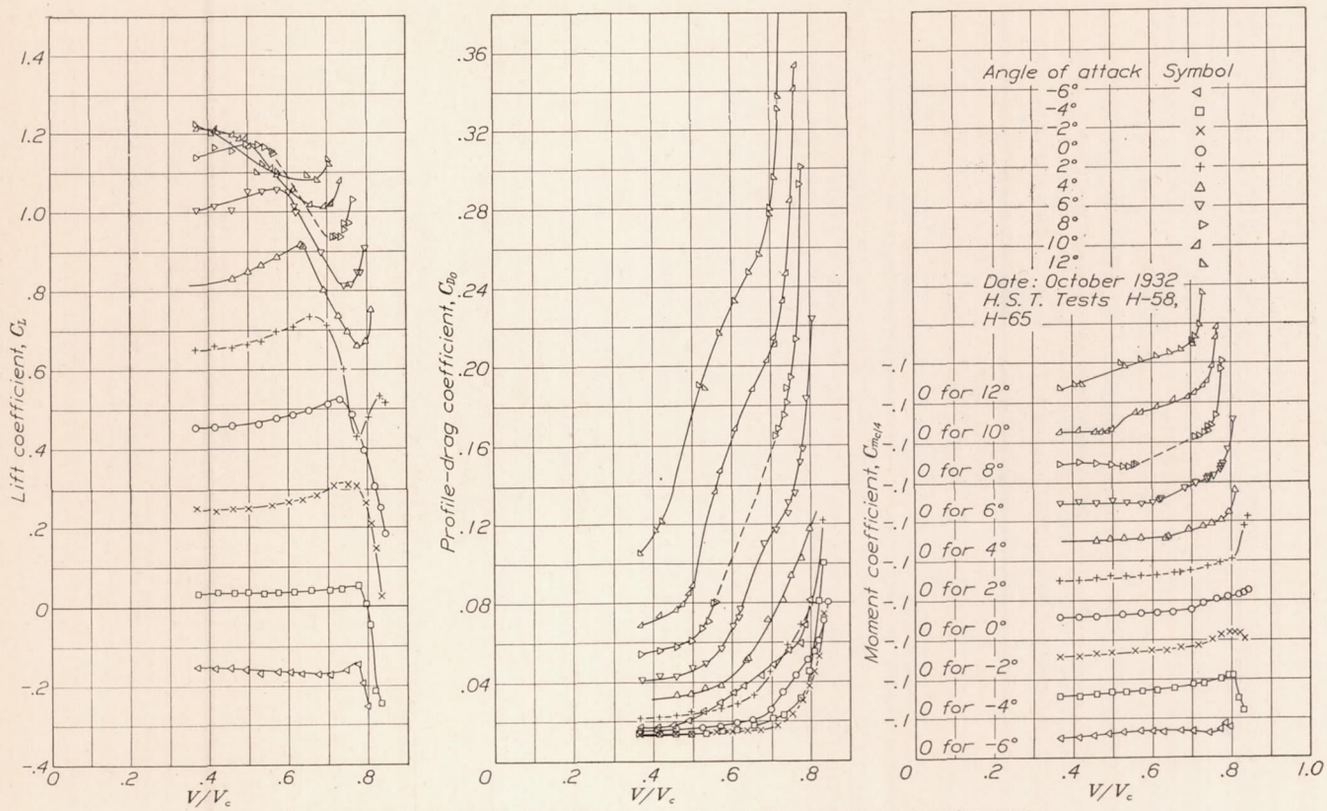

FIGURE 10.—Effects of compressibility on the aerodynamic characteristics of the 3C10 airfoil.

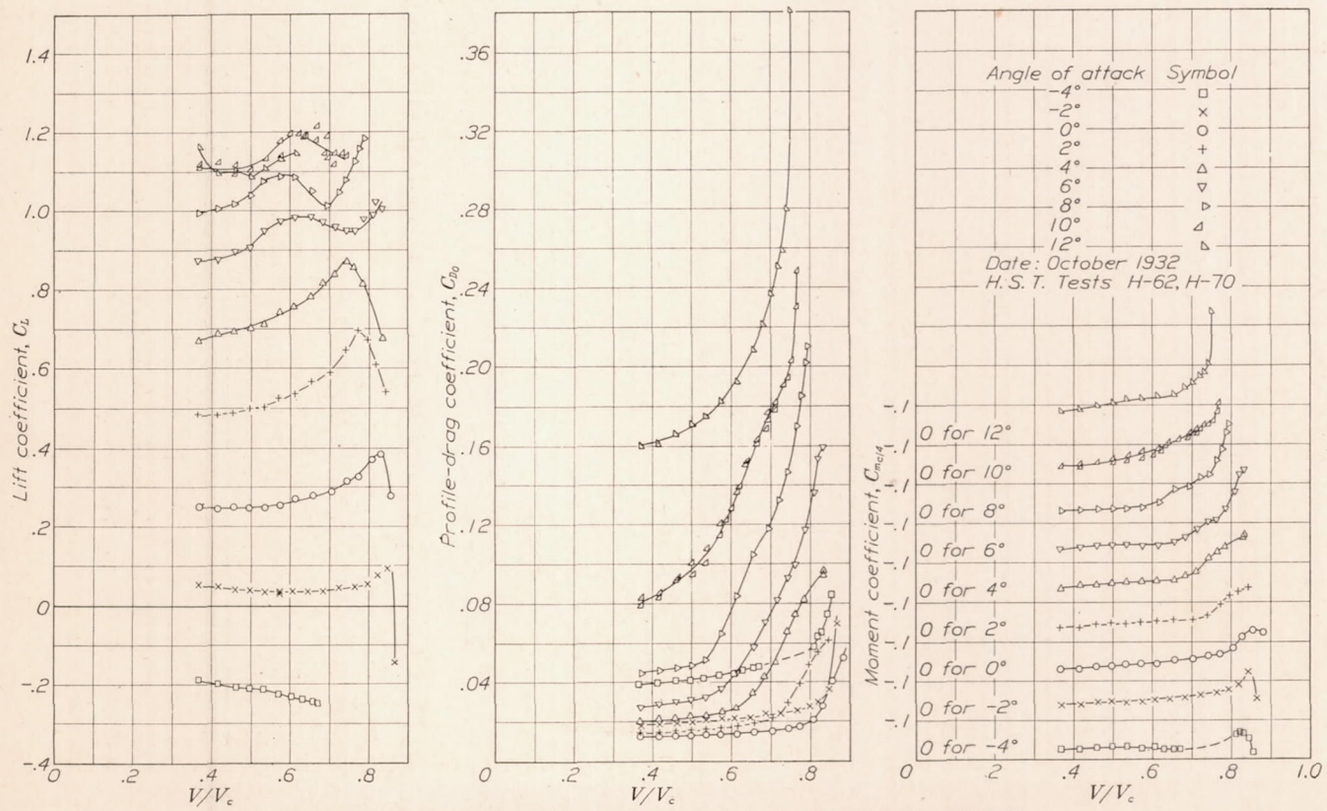

FIGURE 11.—Effects of compressibility on the aerodynamic characteristics of the 3R6 airfoil.

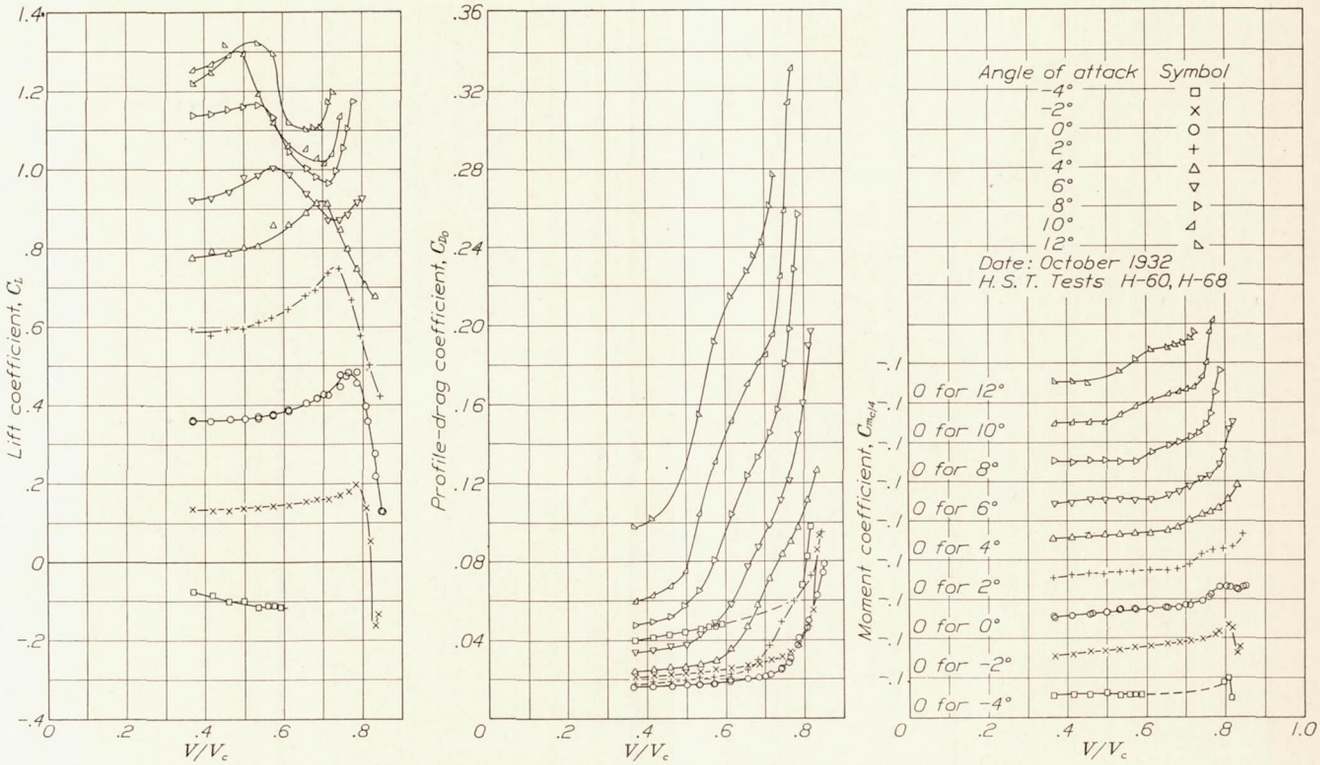

FIGURE 12.—Effects of compressibility on the aerodynamic characteristics of the 3R8 airfoil.

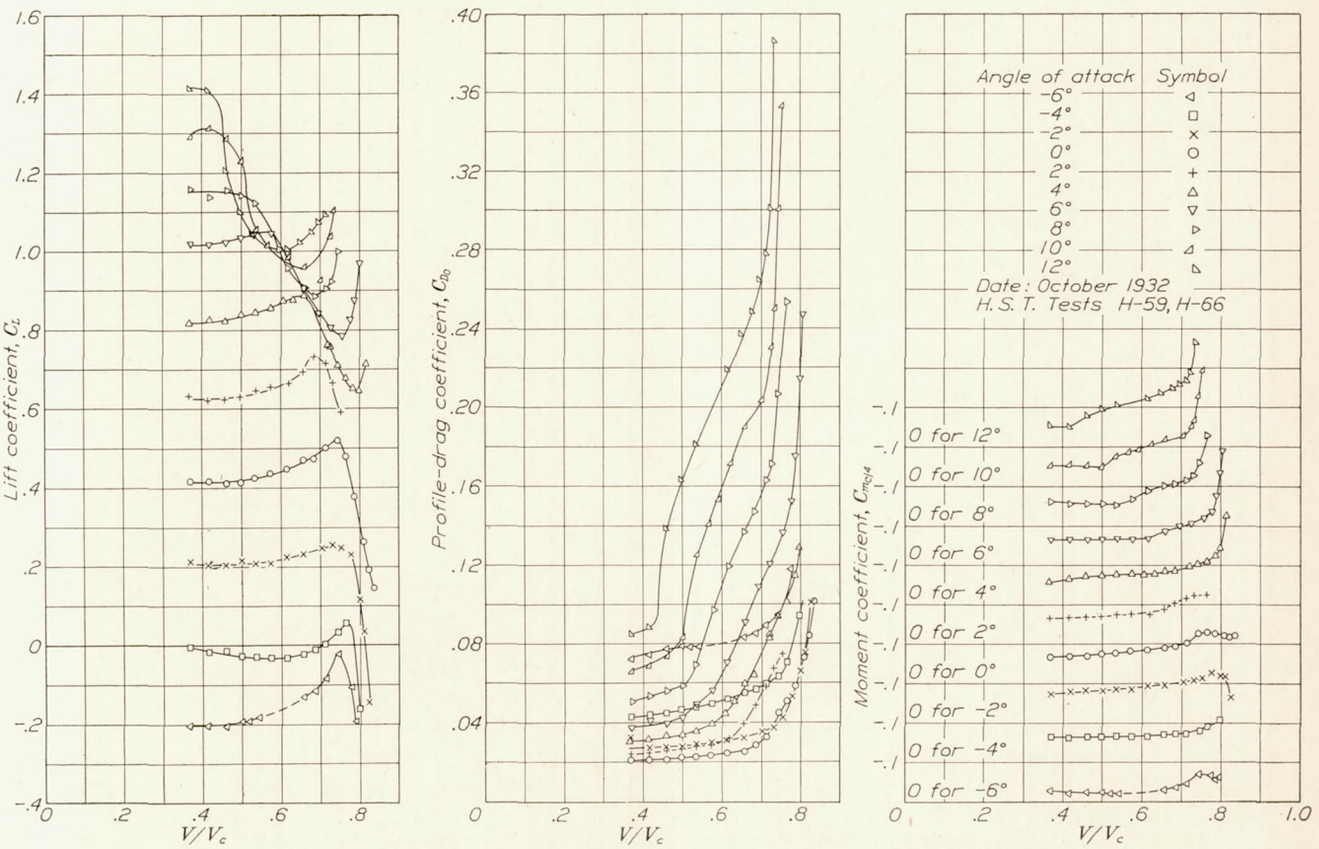

FIGURE 13.—Effects of compressibility on the aerodynamic characteristics of the 3R10 airfoil.

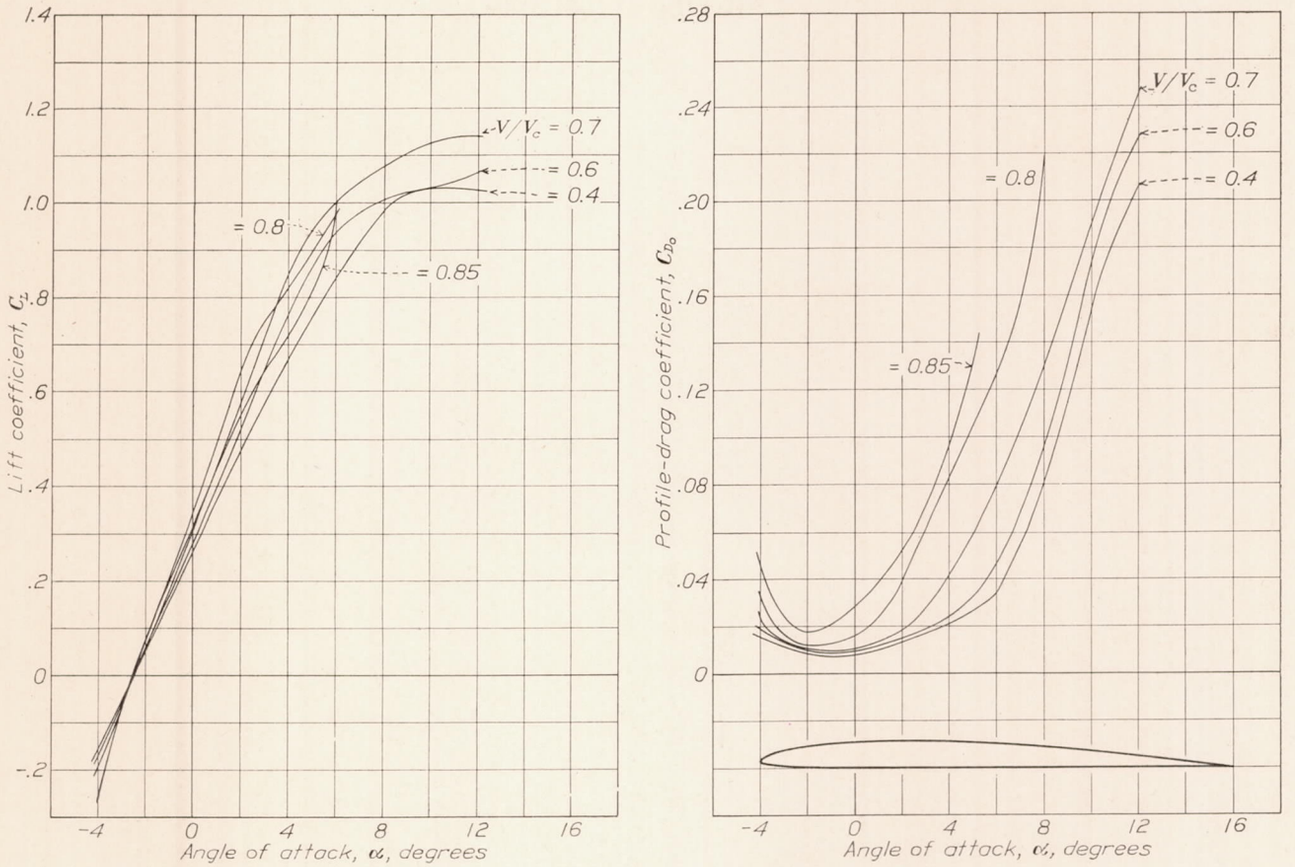

FIGURE 14.—Aerodynamic characteristics of the 3C6 airfoil for various speeds.

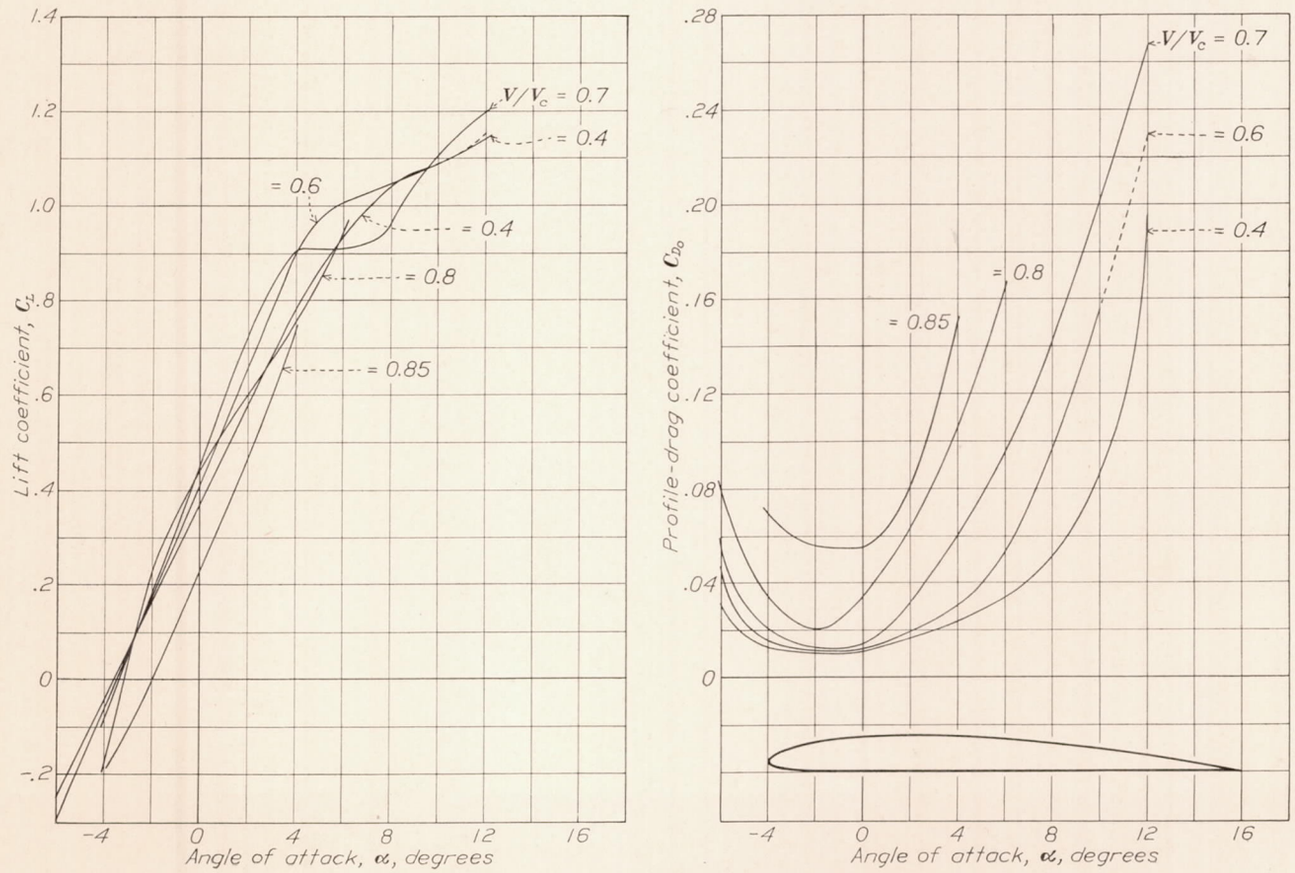

FIGURE 15.—Aerodynamic characteristics of the 3C8 airfoil for various speeds.

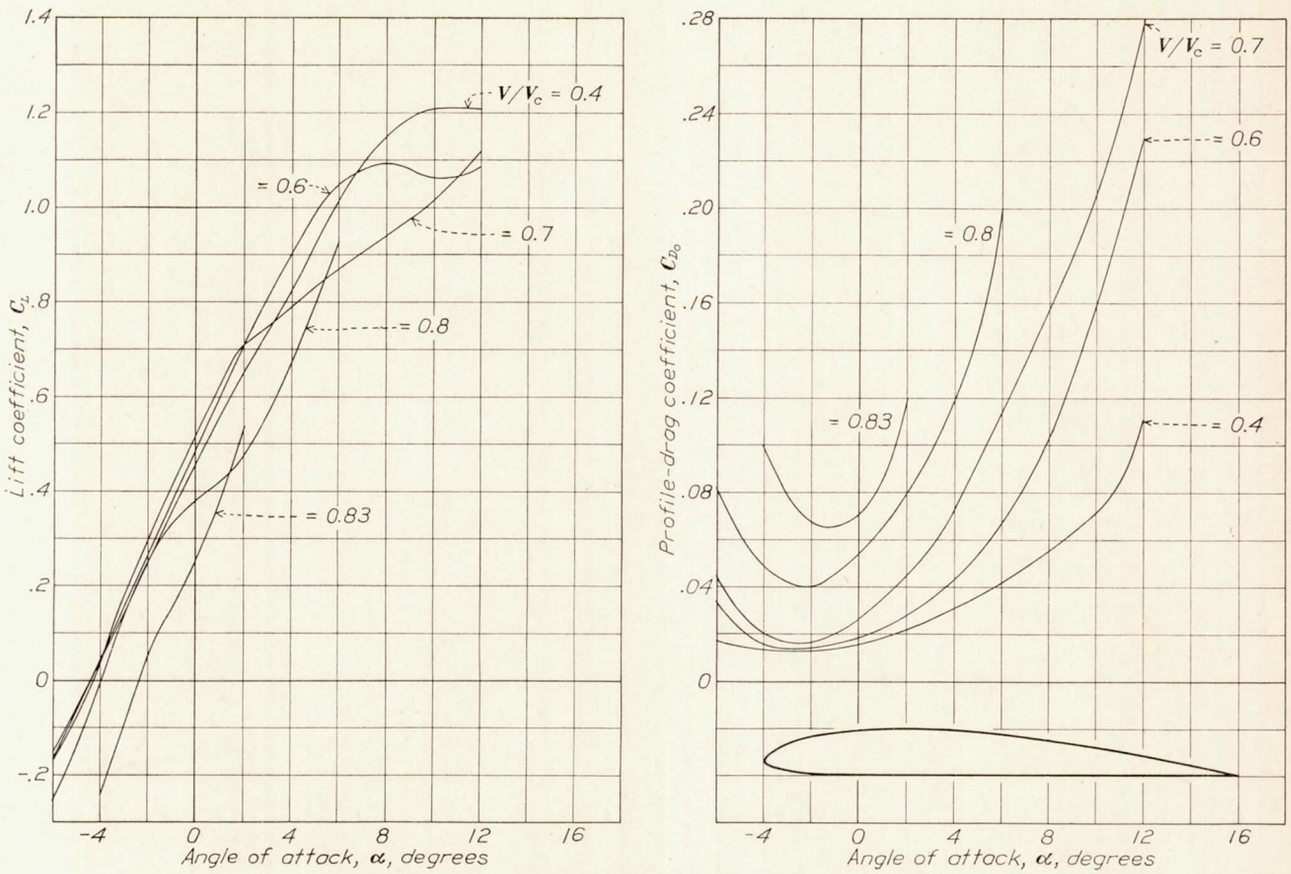

FIGURE 16.—Aerodynamic characteristics of the 3C10 airfoil for various speeds.

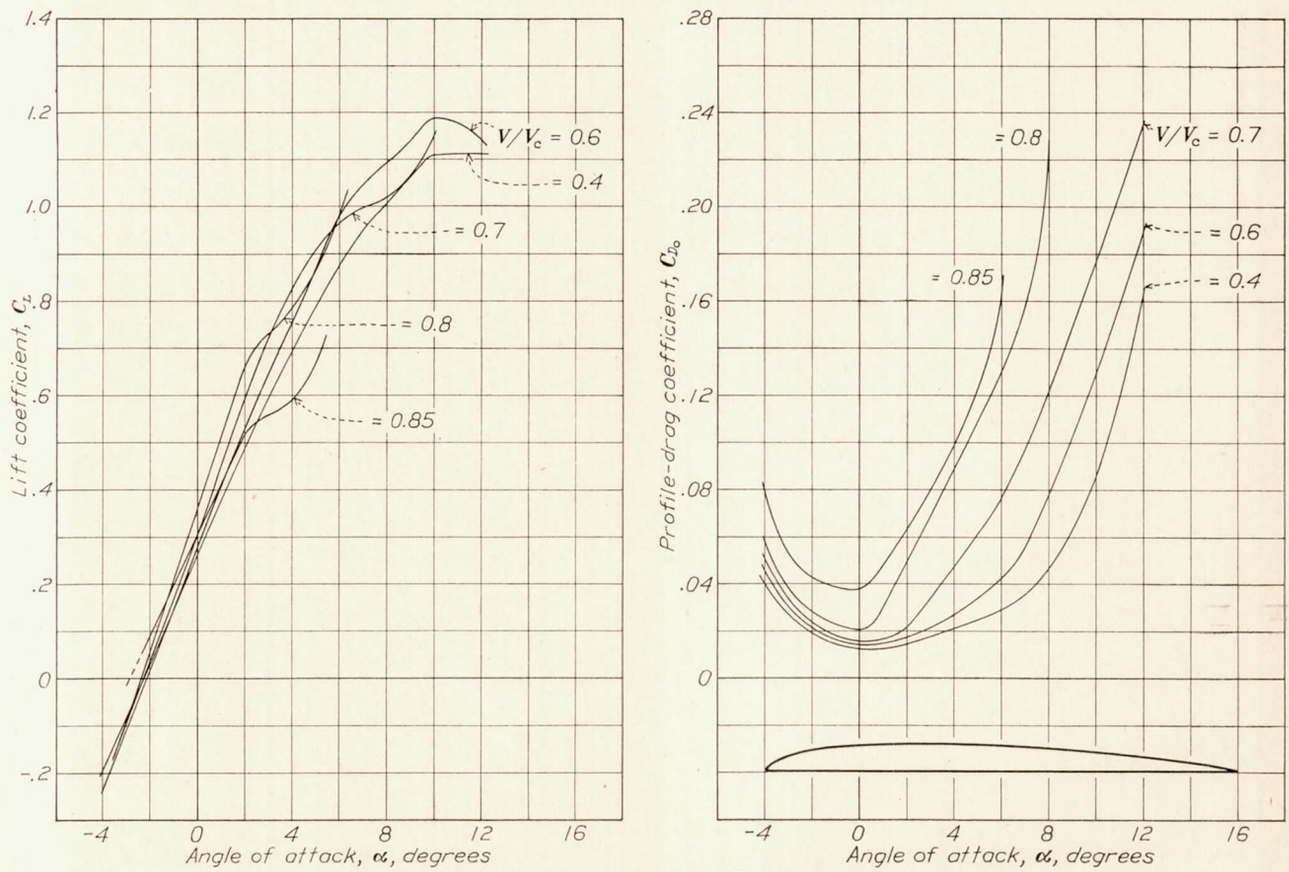

FIGURE 17.—Aerodynamic characteristics of the 3R6 airfoil for various speeds.

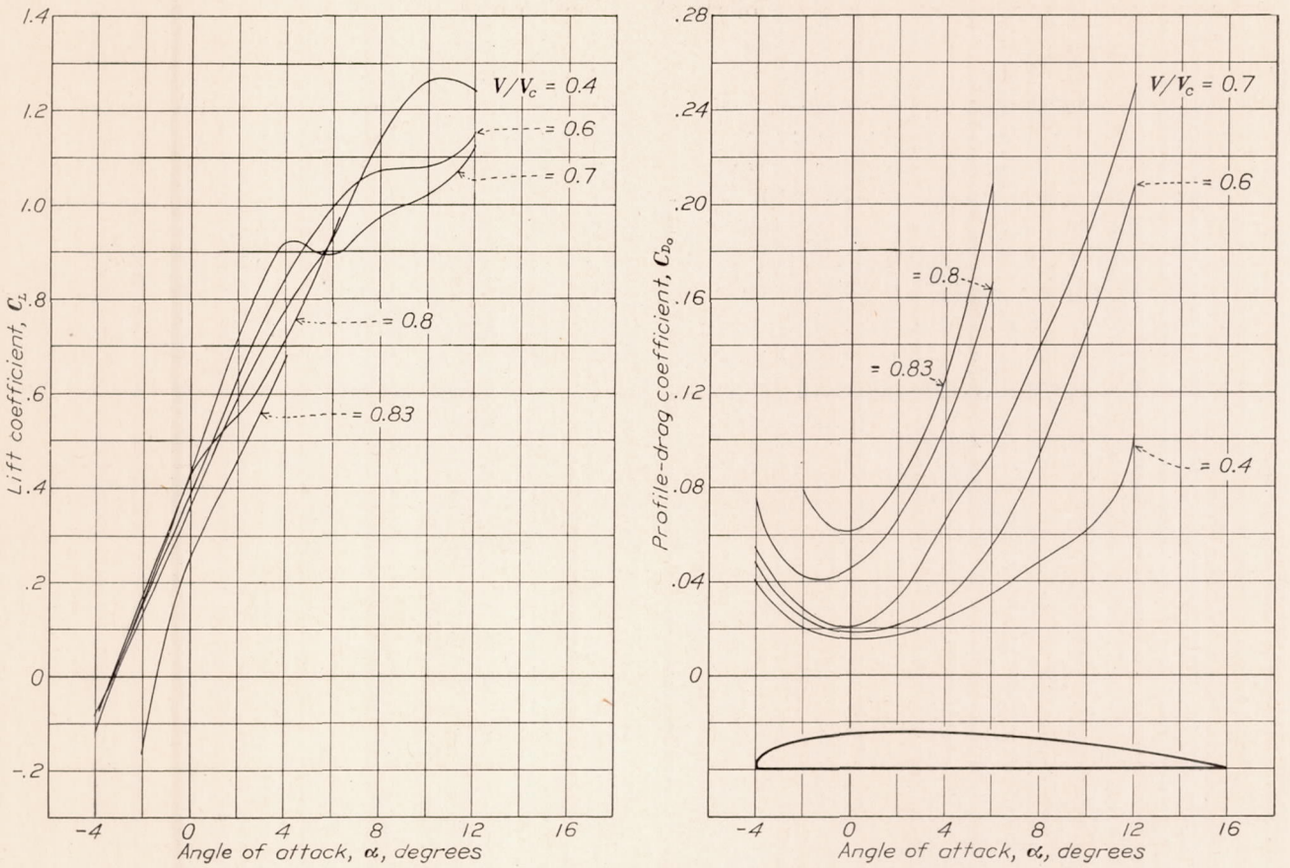

FIGURE 18.—Aerodynamic characteristics of the 3R8 airfoil for various speeds.

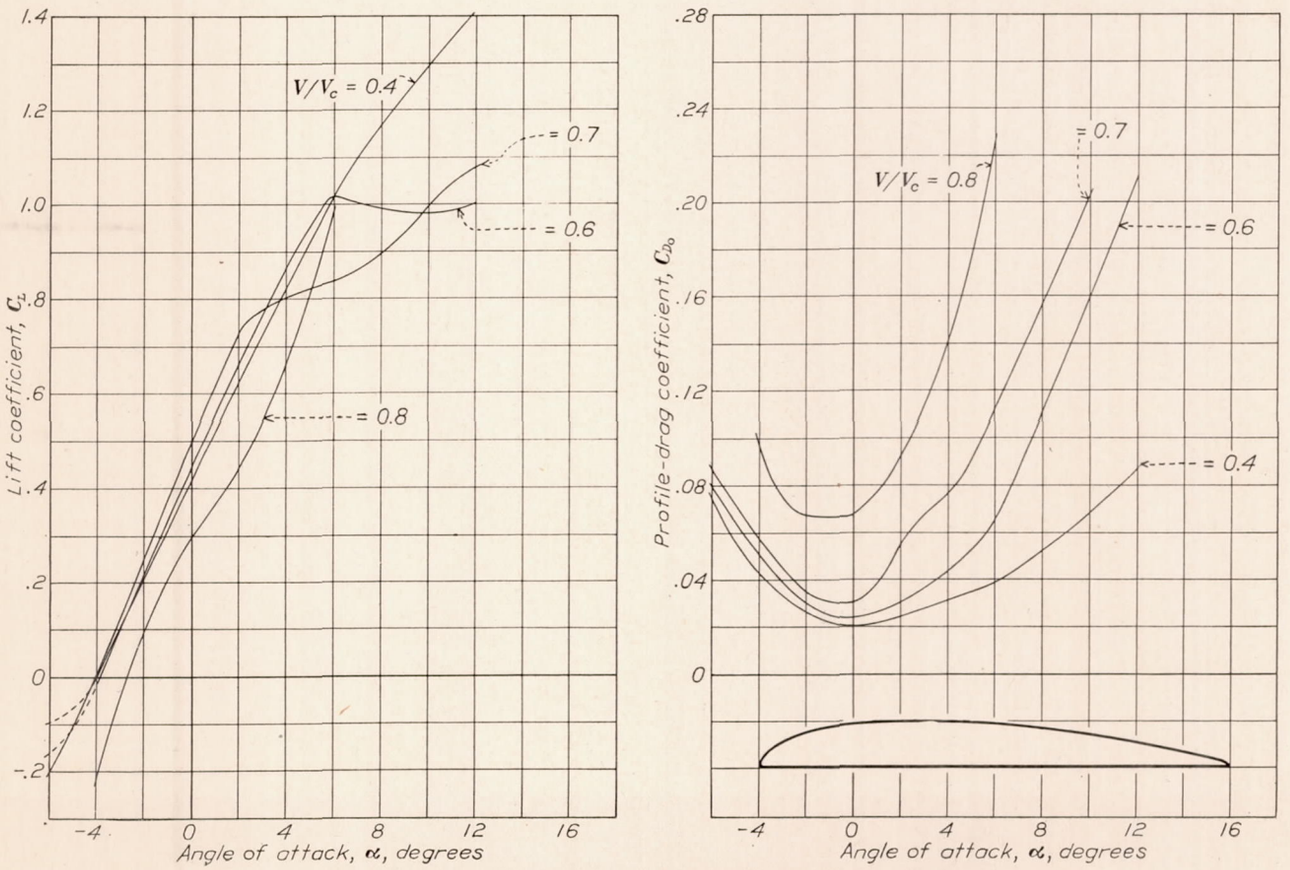

FIGURE 19.—Aerodynamic characteristi... of the 3R10 airfoil for various speeds.

lift curve in the low-drag range) of the R airfoils are slightly higher than the lift-curve slopes for the corresponding C airfoils except for the thickest airfoils. However, the differences are not very great, and, in view of the difficulty of accurately measuring this quantity, no definite conclusions should be drawn.

Variation of the airfoil characteristics with thickness.—Figure 20 shows a uniform increase of minimum-drag coefficients with increasing thickness and, in addition, shows with one exception a like change for the drag coefficient at various values of the lift coefficient. At lower speeds the drag coefficient of the 3C6 airfoil for a lift coefficient of 0.8 is higher than might be expected, which as previously noted is due to the early burble of this C airfoil. The moment coefficient and the angle of zero lift show uniform changes with thickness. These quantities, although not primarily dependent on thickness changes, may be expected to change in a systematic manner because the method employed for varying the airfoil thickness also varies the mean camber. An examination of figures 8 to 13 shows the moment variation with increasing thickness and figures 14 to 19 show the angle of zero-lift variation. The effect of thickness variation on lift-curve slope is not as uniform as the changes of the other aerodynamic properties. However, it is shown in figure 21 that increased thickness, in general, causes a reduction of the lift-curve slope. The maximum lift variations have not been studied in detail because the values of this characteristic are not definite at high speeds.

Effects of compressibility.—As the velocity of the air past the model is increased, pronounced changes occur in the aerodynamic characteristics of the airfoil. These changes are best studied by referring to figures 8 to 13, inclusive. The lift coefficients increase as the speed is increased, slowly as the speed is increased over the lower portion of the range, then more rapidly as speeds above half the velocity of sound are exceeded, and finally at higher speeds, depending on the airfoil

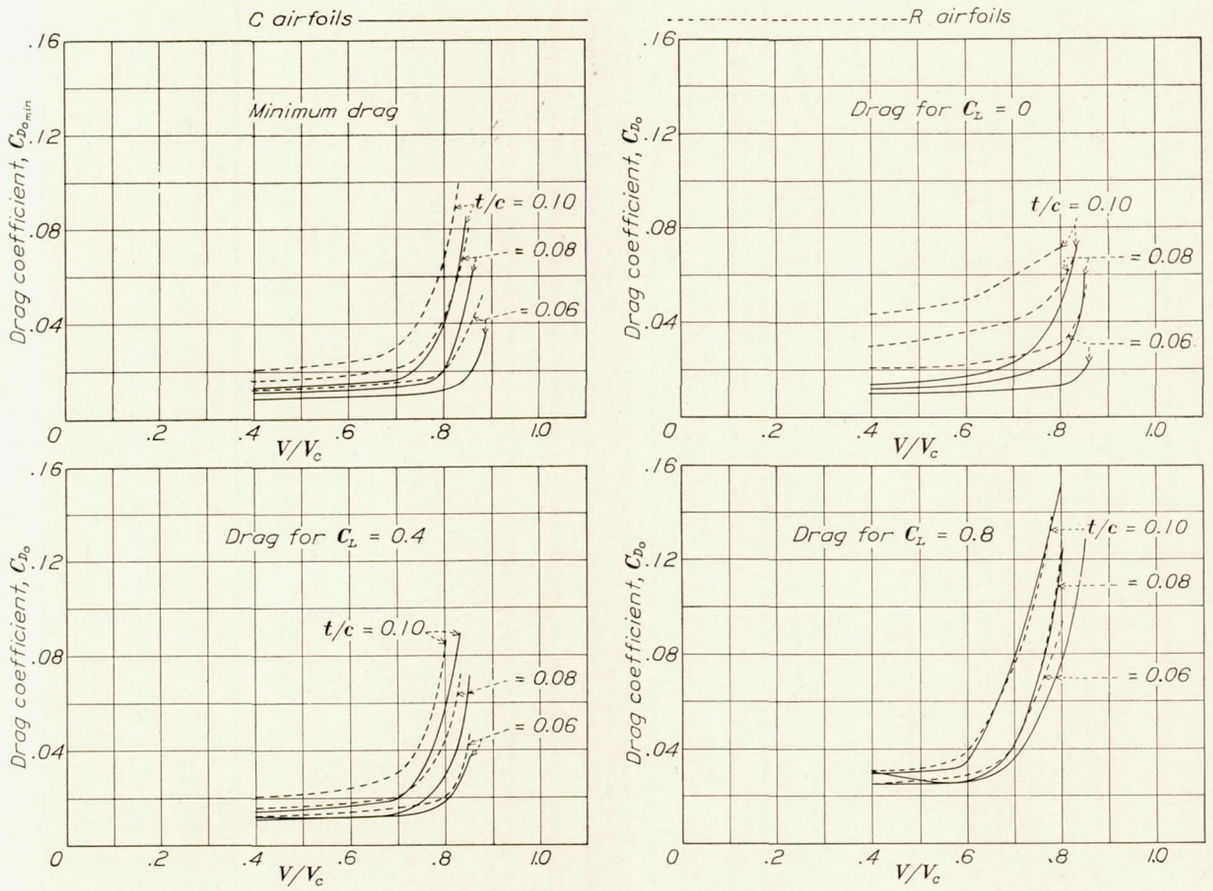

FIGURE 20.—Effect of compressibility on drag.

section and the angle of attack, the flow breaks down as shown by a drop in the lift coefficient. This breakdown of the flow, hereinafter called the compressibility burble, occurs at lower speeds as the lift is increased by changing the angle of attack of the model. At the highest lift coefficients, which are in the region of the normal burble, the breakdown of the flow occurs at low speeds and, because of the unsteadiness of the flow, the curves of lift coefficient plotted against speed become irregular. The drag coefficient behaves in a similar manner. A small but steady increase in drag as the speed is increased is observed, which continues until the compressibility burble is reached. At this point the drag coefficients rise rapidly to values several

times as large as the low-speed values. As with the lift coefficient, the rapid rise in the drag coefficient occurs at lower speeds as the angle of attack is increased until finally, at angles of attack in the neighborhood of

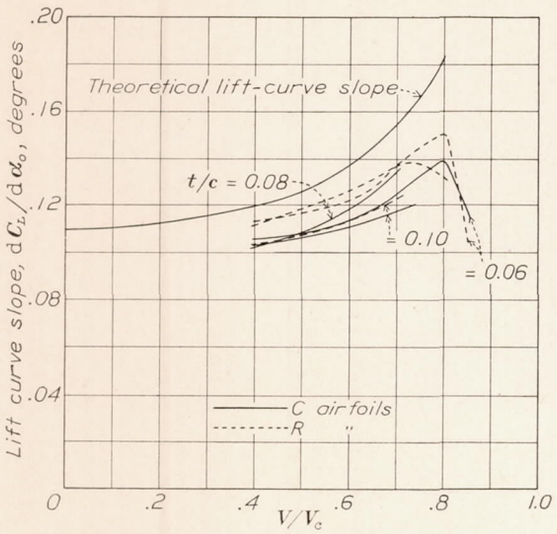

FIGURE 21.—Effect of compressibility on lift.

the normal stall at low speeds, the drag rises rapidly at velocities of the order of 0.4 the velocity of sound. The variation of the moment coefficient is similar to the variation of the lift and drag coefficients. The

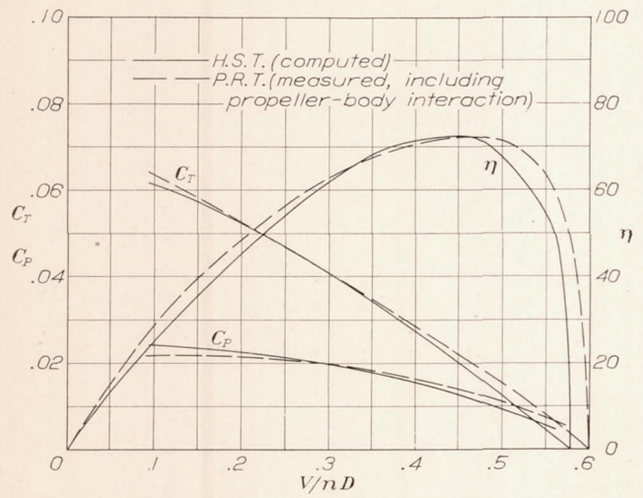

FIGURE 22.—Comparison of computed and measured propeller characteristics—tip speed 0.75 V_c, C-10 propeller.

moment increases numerically as the speed is increased, this change continuing until the compressibility burble is reached. At this point rapid changes in the moment occur.

The effect of compressibility of the moment coefficient is of considerable importance in the structural design of fast-diving airplanes. Speeds in the neighborhood of half the velocity of sound are commonly attained by most airplanes of this type when in a dive, and if low-speed moment data are applied to the design of the spars large errors in the estimation of the distribution of load between the spars may be introduced.

Further changes in the aerodynamic characteristics occur as the speed is increased. The lift-curve slope increases with the speed until a speed corresponding to the general breakdown of the flow is reached. Above this speed the lift curves show either discontinuities or irregularities of form. (See figs. 14 to 19 and fig. 21.) Figures 14 to 19 also show large changes in the angle of zero lift at high speeds. The value is but little affected by speed changes until the compressibility burble occurs. At higher speeds the zero-lift attitude approaches zero angle of attack. The changes are shown in the following table, which has been compiled from figures 14 to 19.

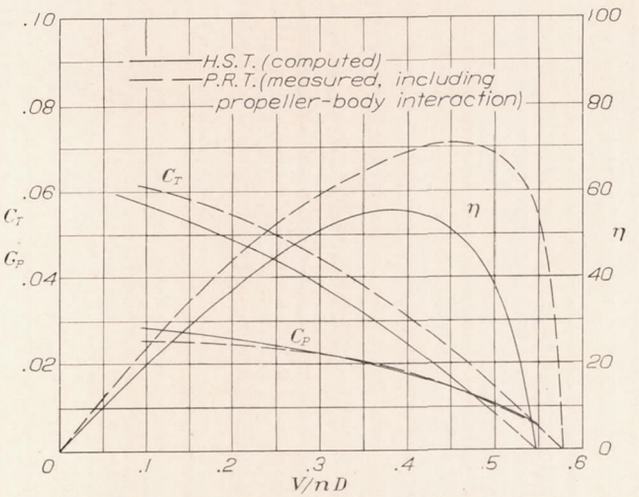

FIGURE 23.—Comparison of computed and measured propeller characteristics—tip speed 0.9 V_c, C-10 propeller.

Airfoil \ V/V_c	0.4	0.6	0.7	0.8	0.83	0.85
	Angle of zero lift					
3C6	−2.5°	−2.45°	−2.45°	−2.5°	----------	−2.55°
3R6	−2.3°	−2.2°	−2.3°	−2.4°	----------	----------
3C8	−3.55°	−3.5°	−3.4°	−3.1°	----------	−1.95°
3R8	−3.2°	−3.2°	−3.25°	−3.3°	−1.45°	----------
3C10	−4.35°	−4.35°	−4.35°	−3.9°	−2.4°	----------
3R10	−4.0°	−3.85°	−4.0°	−2.7°	----------	----------

The shift of the angle of zero lift is not shown by the thinnest airfoils because the compressibility burble at low lifts takes place at speeds slightly higher than those recorded in the table. The results shown in the table, as well as the results shown by figures 20 and 21, lead to the conclusion that the speed at which the compressibility burble occurs is a function of the airfoil thickness. The table shows no change in the angle of zero lift at 85 percent of sound velocity for the thinnest airfoils. The 8 percent thick airfoils show a change in angle of zero lift in the neighborhood of 0.8 V_c and the thickest airfoils show this change occurring at speeds slightly in excess of 0.7 V_c. An examination of the profile-drag coefficient curves for zero lift coefficient (fig. 20) shows the rapid rise in drag occurring at substantially the same values as those previously noted for the angle-of-zero-lift changes.

All the data indicate that the flow breakdown occurs at speeds well below the velocity of sound. The early breakdown of flow is probably due (references 7 and 8) to the fact that the induced velocities over the airfoil are higher than the main-stream velocity and so reach the velocity of sound when the main-stream velocity is much lower than the speed of sound. There are some reasons to believe that the attainment of sound velocity at any point in the field of flow causes a marked change in the type of flow and is probably responsible for the compressibility burble. The experimental data tend to substantiate this deduction. The compressibility burble, as indicated by the peaks of the curves of the lift coefficient plotted against V/V_c for various angles of attack (figs. 8 to 13), occurs at lower speeds as the angle of attack or the lift is increased. The shift of the angle of zero lift following the compressibility burble is attributed to the reduction in lift over the upper surface of the airfoil which occurs concurrently with the flow breakdown.

Theoretical investigations of the effects of compressibility have so far yielded but little information regarding the actual flow phenomena, principally because of mathematical complications arising in the analysis. Rayleigh and Bryan (references 9, 10, and 11) have attempted solutions but the mathematical complication involved in the application of their work seems to have virtually prohibited the solution of any practical problem. More recently Taylor, Glauert, and Ackeret (references 12, 13, and 14) have attempted solutions and have to some extent succeeded in predicting some of the effects that have been observed experimentally. The mechanical method for solving fluid flow as devised by Taylor (reference 12) indicates that a change in the type of flow occurs when the velocity at any place in the field of flow, and not necessarily the velocity of the main stream, attains the velocity of sound. This work is of importance in that it points to definite limitations in the theoretical analysis of Glauert and Ackeret. The success of the mechanical method for solving fluid flows depends on an analogy between the equations for the irrotational motion of a fluid and the equations for the flow of electric current in a sheet of conducting substance of variable depth, an electrolyte in Taylor's experiments. As the experiments with the electric analogy progressed, it became apparent that no solution could be obtained if the veloc ty of the fluid at any point in the field of flow equaled or exceeded the velocity of sound. This fact leads to the inference that irrotational motion, the type of flow postulated by Glauert and Ackeret, does not exist if sound speed is reached at any point in the field of flow. Taylor's experiments on the 12¼ percent thick R.A.F. 31a airfoil indicate a change in type of flow at a main-stream velocity between 0.5 V_c and 0.65 V_c when the attitude of the airfoil is such that the low-speed lift coefficient is n the neighborhood of 0.8. The present work indicates that a breakdown of the flow occurs at a speed of approximately 0.64 V_c for the thicker airfoils when their attitude is the same as that of the R.A.F. 31a in Taylor's experiments. It would seem, therefore, in view of the agreement of the direct experimental and mechanical methods of measurement regarding the breakdown in flow, that any theoretical analysis of the effect of compressibility postulated on irrotational motion is inapplicable at relatively high speeds.

This limitation is imposed on the theoretical work of Glauert and Ackeret. In addition, Glauert's work is further restricted because it assumes that the velocity at the surface of the airfoil does not differ appreciably from the main-stream velocity. Ackeret's method of analysis differs somewhat from Glauert's, but it also is subject to the same restrictions. Both agree, however, on the change which might be expected in the early stages. The important conclusion reached by both is that the lift-curve slope may be expected to vary proportionately with the factor $(1-(V/V_c)^2)^{-\frac{1}{2}}$. In order to verify this prediction the theoretical lift-curve slope variation has been plotted against V/V_c with the experimental results in figure 21. The similarity of the experimental curves to the theoretical curve is striking and leads to the conclusion that at speeds below that at which the compressibility burble occurs, the application of the factor to the known experimental lift-curve slope at low speeds is justified for practical purposes.

Glauert's work also indicates that the chord of the airfoil in a compressible flow is effectively shorter than the chord of the airfoil in an incompressible flow. The effect of compressibility is then to increase the effective camber of the airfoil and as a result the moment coefficient may be expected to increase numerically. The moment-coefficient curves (figs. 8 to 13) show a change in the same direction as that predicted.

Comparison with previous work.—Airfoils similar to those studied in this investigation, as well as other airfoils, have been tested previously over a wide speed range but the results of the earlier investigations are not directly comparable with these results because of different test conditions. The earliest experimental investigation of airfoil characteristics as affected by compressibility is described in reference 15. Similar airfoils were later tested (reference 16) over a wider speed range in a different form of wind tunnel. Pressure-distribution test of these airfoils were also made (reference 7) but quantitative correlation with previous results was again impossible because of different test conditions. The latest measurements are those given in reference 5. None of the foregoing investigations, however, affords a quantitative comparison with the present investigation. The tests of reference 15 consisted only of lift measurements of six airfoils of 1-inch chord and 6-inch span mounted on a central support in a 14-inch diameter wind tunnel. The results are

of limited value because of the small speed range and the low Reynolds Number. The tests described in reference 16 were made in an open-jet wind tunnel. The models were of 3-inch chord; they extended across a jet of air issuing from a 12.24-inch nozzle and projected into the still-air region on either side of the jet. The air mixed directly with the atmosphere. The tests described in references 5 and 7 were made in a similar tunnel but the diameter of the air jet was 2 inches and the chord of the models was 1 inch. These results are, of course, subject to large aspect-ratio corrections and because of the unknown influence of the jet boundaries and model end conditions, these corrections are unknown. The results are therefore comparable only qualitatively with the results of this investigation. Some tests of other airfoils have been made in England under approximately infinite aspect-ratio conditions in a small wind tunnel so that although the tunnel-boundary conditions are satisfactory the Reynolds Number for the tests is much smaller than that obtained in the present investigation.

An examination of the effects of compressibility on airfoil characteristics as demonstrated by the earlier investigations does show good agreement, qualitatively, with the results of the present investigation. The existence of a definite compressibility burble has been shown and the speed at which this occurs has been shown to be influenced by the airfoil thickness and the angle of attack of the airfoil (reference 16). The marked drag increase has also been demonstrated. The gradual change in the moment coefficients for speed changes below the speed at which the compressibility burble occurs has not been shown previously. This difference may be explained by the inherent inaccuracy of the methods previously used for measuring this quantity (reference 16). The systematic change in the lift-curve slope has been shown by the British tests (reference 17), but not by previous American tests, which is undoubtedly due to the large influences of the boundaries of the air jet used in the American tests on the character of the flow over the airfoil. An important difference between the present tests and those of reference 5 concerns the relative advantages of C and R airfoils. The results of reference 5 indicate that for airfoil thicknesses less than $0.1c$ the R airfoils are superior to the C airfoils at high angles of attack. For thickness ratios of 0.08 or larger the difference between the C and R airfoils at high angles of attack is shown by these tests to be small, but the C airfoils are, in general, slightly better. Because the differences are small, it may be that the relatively large effects of the jet boundaries in the earlier tests influenced the results. Another difference in the results of these and previous tests which may be attributed to jet-boundary phenomena is found in the speeds at which the compressibility burble occurs. The shift of the angle of zero lift at very high speeds is substantiated and the advantages of using thin sections in preference to thick sections at high speeds are also substantiated.

Computation of propeller characteristics.—The six airfoils tested in this investigation are used chiefly as propeller blade sections, and one of the purposes of this investigation was to provide better data than have heretofore been available on the aerodynamic properties of these sections. In order to demonstrate the extent to which the results of this investigation may be directly applied to practical propeller design, the characteristics of a propeller on which tests for a wide range of tip speeds are available have been computed from these data.

The propeller chosen is the C-10 propeller of reference 18. The blade sections of this propeller are 3C10 sections. The pitch of the propeller is 9.6° at the 0.75 radius. The propeller characteristics have been computed from the section data by means of the improved vortex theory of Goldstein (reference 19). The equations used have been taken from this reference and modified so that the standard nondimensional coefficients in use in this country may be used directly in the formulas. The expression for the differential thurst is

$$R\frac{dC_T}{dr}=\frac{1}{4}\left(\frac{r}{R}\right)^3\pi^3\delta(1-a_2)^2\lambda_1\sec^2\varphi \qquad (1)$$

The differential torque is obtained from the formula

$$R\frac{dC_Q}{dr}=\frac{1}{8}\left(\frac{r}{R}\right)^4\pi^3\delta(1-a_2)^2\lambda_2\sec^2\varphi \qquad (2)$$

The rate of advance is given by

$$V/nD=\pi\left(\frac{r}{R}\right)(1-a_2)(1-F)\tan\varphi \qquad (3)$$

where the factors F and a_2 are obtained from the following expressions

$$F=\frac{\cos^2\varphi}{K}\frac{\delta}{4}\frac{\lambda_1}{\sin^2\varphi} \qquad (4)$$

$$\frac{a_2}{1-a_2}=\frac{\cos^2\varphi}{K}\frac{\delta}{2}\frac{\lambda_2}{\sin 2\varphi} \qquad (5)$$

and the following are the symbols used:

φ, the angle between the path of a blade element and the plane of rotation

$\delta=\dfrac{Bc}{2\pi r}$

R, tip radius

r, section radius

B, number of blades

c, chord of blade section

$\lambda_1=C_L\cos\varphi-C_D\sin\varphi$

$\lambda_2=C_L\sin\varphi+C_D\cos\varphi$

K, a coefficient dependent on r/R, B, and φ

These expressions are identical with those given by the vortex theory with the exception of the factor

$\cos^2\varphi/K$ in the expressions for a_2 and F. In order to facilitate application of the foregoing equations a chart giving values of $K/\cos^2\varphi$ for 2-bladed propellers plotted against tan φ is given as figure 24. This chart has been taken from reference 19. It is worth noting in passing that the factor $\cos^2\varphi/K$ becomes unity if the number of blades is infinite. The vortex theory assumes that the number of blades is infinite and the agreement of the new theory with the vortex theory is complete for this condition.

The actual calculation was carried out in the usual manner. The differential thrust and torque coefficients and rate of advance were computed from the foregoing formulas. The coefficients were plotted against V/nD and from these plots the thrust and torque grading curves were constructed for various values of V/nD. The grading curves were integrated mechanically to obtain the over-all coefficients of the propeller. The computation was carried out for two tip speeds, $0.75V/V_c$ and $0.9V/V_c$. The airfoil coefficients were taken from figure 10. Calculations

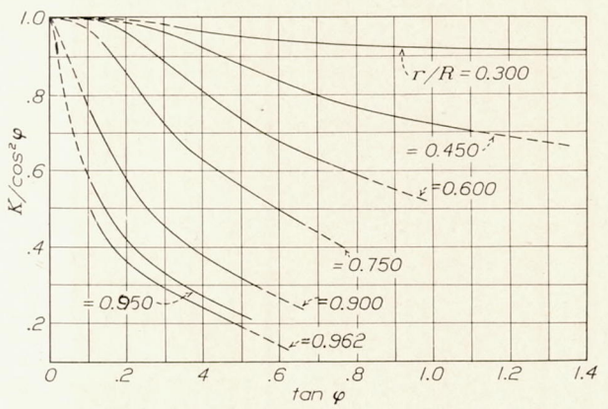

FIGURE 24.—Goldstein factor for correcting the vortex theory for 2-bladed propellers (reproduced from British R. & M. No. 1377).

were made for even 2° intervals of angle of attack. The speed of the various propeller sections was taken as the product of the tip speed and the ratio of the section radius to the tip radius. A slight error is introduced in this way because the resultant speed at any section is not exactly proportional to the radius, owing to the forward speed. The error is small, however, for low pitches; in the present instances it is of the order of 1.3 percent for the highest rates of advance.

The propeller characteristics as computed from these data and the measured propeller characteristics, taken from reference 18, are plotted in figures 22 and 23. In view of the fact that the measured propeller characteristics are influenced by the effects of the hub drag and the propeller-body interaction, exact agreement cannot be expected. Previous experience, however, indicates that the net interference effect is small because the effects of the hub drag and the additional drag of the body due to slipstream tend to compensate the effects of the body on the propeller characteristics, so that a comparison of the computed and the measured propeller characteristics may be expected to yield information of some value.

The important difference between the computed and the measured characteristics is in the value of the thrust coefficient when the tip speed is equal to 0.9 V_c. This difference causes a marked reduction in the propeller efficiency as deduced from the airfoil data. Apparently, the maximum efficiency from the computed characteristics begins to fall off at lower tip speeds than the corresponding efficiency from the measured characteristics.

There are several possible causes for the disagreement at the high tip speed. The most important factors contributing to the difference are probably Reynolds Number differences and a constriction at the test section of the high-speed tunnel when the model is in position. Tests made in England of model propellers have shown a drop in efficiency at speeds lower than that shown by the full-scale tests. This difference between the model and full-scale tests has been attributed to Reynolds Number differences. The Reynolds Number of both the present tests and the British model propeller tests giving similar results is in the neighborhood of half that attained in the full-scale propeller tests of reference 18.

A constriction effect at the test section due to the presence of the model would also tend to cause a difference in the same direction as that shown in figure 23. In substance, the velocity and q as determined from the static-plate measurements would be lower than the effective velocity and q at the throat. As a result, the observations plotted in figures 8 to 13 would be plotted at speeds slightly lower than the correct values and the coefficients would be somewhat larger than the true values. The magnitude of the constriction or blocking correction would probably be greater for high speeds and high angles of attack than for low speeds and low angles of attack.

A thorough investigation of the causes of the discrepancy would require considerable additional experiment. The variation of the maximum efficiency of a propeller with tip speed should first be studied by means of flight tests to verify or disprove the results of the tests in the propeller-research tunnel. The effects of the body behind the propeller (a fuselage housing a D-12 engine in the tests of reference 18) should be investigated by means of tests of the propeller without a body. The effects of Reynolds Number should be investigated by means of tests of a geometrically similar model in the propeller-research tunnel. The blocking or constriction correction for the high-speed tunnel results cannot be investigated with the equipment now available. The method of determining this correction consists of testing geometrically similar airfoils of different chord. If this were to be done in the equipment now available the Reynolds Number would vary

as well as the constriction at the throat. A method suitable for establishing this correction is the construction of a high-speed wind tunnel similar to the present tunnel, but different in size, and the testing in both tunnels of airfoils of the same chord. The Reynolds Number would then be the same for the tests in each tunnel but the effects of constriction would depend on the sizes of the tunnels. One additional recommendation, but one which at present seems to offer but little possibility of success, is a theoretical analysis of the flow in the tunnel with a view to determining the constriction correction. The analysis should include an examination of the effects of compressibility. This stipulation is important but, because of the mathematical difficulty involved, a solution by this means seems improbable.

CONCLUSIONS

1. Clark Y airfoil sections are superior to R.A.F. 6 airfoil sections for propeller applications except for high-pitch propellers operating at low values of V/nD.

2. For propellers rotating at very high speeds, thin sections are better than thick sections.

3. As the speed of the air flowing past an airfoil is increased the lift, drag, and moment coefficients undergo a small numerical increase which continues until a compressibility burble occurs.

4. As the speed is further increased the breakdown of the flow corresponding to the compressibility burble is evidenced by a drop in the lift coefficient and a rapid increase in the drag coefficient.

5. The speed at which the compressibility burble occurs is dependent on the angle of attack and the thickness of the airfoil; increasing either of these causes the compressibility burble to occur at lower speeds.

6. Although the Reynolds Numbers at which these tests were conducted are low the results indicate that errors may be expected in the estimated design loads for airplanes which attain speeds such as those attained by diving bombers when in a dive if the effects of compressibility on the wing moment coefficient are neglected.

7. These results indicate that the limited theory available may be applied with sufficient accuracy for most practical purposes only for speeds below the compressibility burble.

LANGLEY MEMORIAL AERONAUTICAL LABORATORY,
NATIONAL ADVISORY COMMITTEE FOR AERONAUTICS,
LANGLEY FIELD, *March 28, 1933.*

REFERENCES

1. Jacobs, Eastman N., and Shoemaker, James M.: Tests on Thrust Augmentors for Jet Propulsion. T.N. No. 431, N.A.C.A., 1932.
2. Glauert, H.: The Elements of Aerofoil and Airscrew Theory. Cambridge University Press, 1926.
3. Norton, F. H.: N.A.C.A. Recording Air Speed Meter. T.N. No. 64, N.A.C.A., 1921.
4. Jacobs, Eastman N., and Abbott, Ira H.: The N.A.C.A. Variable-Density Wind Tunnel. T.R. No. 416, N.A.C.A. 1932.
5. Briggs, L. J., and Dryden, H. L.: Aerodynamic Characteristics of Twenty-Four Airfoils at High Speeds. T.R. No. 319, N.A.C.A., 1929.
6. Freeman, Hugh B.: Comparison of Full-Scale Propellers Having R.A.F. 6 and Clark Y Airfoil Sections. T.R. No, 378, N.A.C.A., 1931.
7. Briggs, L. J., and Dryden, H. L.: Pressure Distribution over Airfoils at High Speeds. T.R. No. 255, N.A.C.A., 1927.
8. Taylor, G. I.: Report on Progress during 1927–28 in Calculation of Flow of Compressible Fluid, and Suggestions for Further Work. R. & M. No. 1196, British A.R.C., 1929.
9. Rayleigh, Lord: On the Flow of Compressible Fluid Past an Obstacle. Philosophical Magazine, vol. 32, July 1916, pp. 1–6.
10. Bryan, G. H.: The Effect of Compressibility on Stream Line Motions. R. & M. No. 555, British A.C.A., 1918.
11. Bryan, G. H.: The Effect of Compressibility on High Speed Stream Line Motions. Part II. R. & M. No. 640, British A.C.A., 1919.
12. Taylor, G. I., and Sharman, C. F.: A Mechanical Method for Solving Problems of Flow in Compressible Fluids. R. & M. No. 1195, British A.R.C., 1928.
13. Glauert, H.: The Effect of Compressibility on the Lift of an Aerofoil. R. & M. No. 1135, British A.R.C., 1927.
14. Ackeret, J.: Über Luftkräfte bei sehr grossen Geschwindigkeiten insbesondere bei ebenen Strömungen. Helvetica Physica Acta, vol. I, Fasciculus Quintus, 1928.
15. Caldwell, F. W., and Fales, E. N.: Wind Tunnel Studies in Aerodynamic Phenomena at High Speed. T.R. No. 83, N.A.C.A., 1920.
16. Briggs, L. J., Hull, G. F., and Dryden, H. L.: Aerodynamic Characteristics of Airfoils at High Speeds. T.R. No. 207, N.A.C.A., 1925.
17. Stanton, T. E.: A High Speed Wind Channel for Tests on Aerofoils. R. & M. No. 1130, British A.R.C., 1928.
18. Wood, Donald H.: Full-Scale Tests of Metal Propellers at High Tip Speeds. T.R. No. 375, N.A.C.A., 1931.
19. Lock, C. N. H.: Application of Goldstein's Airscrew Theory to Design. R. & M. No. 1377, British A.R.C., 1932.

TABLE I

AIRFOIL ORDINATES

[NOTE.—All values in percent of chord]

Station	3C6		3C8		3C10		3R6		3R8		3R10	
	Upper surface	Lower surface	Upper surface	Lower surface	Upper surface	Lower surface	Upper surface	Lower surface	Upper surface	Lower surface	Upper surface	Lower surface
0	1.79	1.79	2.39	2.39	2.99	2.99						
1.25	2.80	.99	3.73	1.32	4.66	1.65						
2.5	3.33	.75	4.44	1.00	5.56	1.26	2.46	0.00	3.28	0.00	4.10	0.00
5	4.05	.48	5.40	.64	6.75	.80	3.54	.00	4.72	.00	5.90	.00
7.5	4.54	.32	6.05	.43	7.56	.54	4.23	.00	5.66	.00	7.08	.00
10	4.92	.22	6.56	.29	8.20	.36	4.74	.00	6.32	.00	7.90	.00
15	5.48	.08	7.31	.10	9.14	.13	5.37	.00	7.16	.00	8.95	.00
20	5.82	.02	7.77	.02	9.72	.03	5.70	.00	7.60	.00	9.50	.00
30	6.00	.00	8.00	.00	10.00	.00	5.99	.00	7.98	.00	9.98	.00
40	5.85	.00	7.80	.00	9.75	.00	5.94	.00	7.92	.00	9.90	.00
50	5.40	.00	7.20	.00	9.00	.00	5.70	.00	7.60	.00	9.50	.00
60	4.69	.00	6.26	.00	7.82	.00	5.22	.00	6.96	.00	8.70	.00
70	3.77	.00	5.03	.00	6.28	.00	4.44	.00	5.92	.00	7.40	.00
80	2.68	.00	3.57	.00	4.46	.00	3.36	.00	4.48	.00	5.60	.00
90	1.44	.00	1.91	.00	2.39	.00	2.11	.00	2.82	.00	3.52	.00
95	.76	.00	1.02	.00	1.27	.00	1.48	.00	1.97	.00	2.46	.00
100	.06	.00	.08	.00	.10	.00						
L. E. Rad.							.60		.80		1.00	
T. E. Rad.							.46		.62		.92	

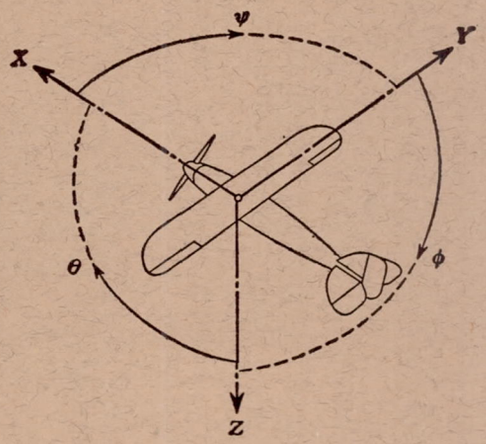

Positive directions of axes and angles (forces and moments) are shown by arrows

Axis		Force (parallel to axis) symbol	Moment about axis			Angle		Velocities	
Designation	Symbol		Designation	Symbol	Positive direction	Designation	Symbol	Linear (component along axis)	Angular
Longitudinal	X	X	rolling	L	$Y \longrightarrow Z$	roll	ϕ	u	p
Lateral	Y	Y	pitching	M	$Z \longrightarrow X$	pitch	θ	v	q
Normal	Z	Z	yawing	N	$X \longrightarrow Y$	yaw	ψ	w	r

Absolute coefficients of moment

$$C_l = \frac{L}{qbS} \qquad C_m = \frac{M}{qcS} \qquad C_n = \frac{N}{qbS}$$

Angle of set of control surface (relative to neutral position), δ. (Indicate surface by proper subscript.)

4. PROPELLER SYMBOLS

D, Diameter.

p, Geometric pitch.

p/D, Pitch ratio.

V', Inflow velocity.

V_s, Slipstream velocity.

T, Thrust, absolute coefficient $C_T = \frac{T}{\rho n^2 D^4}$

Q, Torque, absolute coefficient $C_Q = \frac{Q}{\rho n^2 D^5}$

P, Power, absolute coefficient $C_P = \frac{P}{\rho n^3 D^5}$.

C_s, Speed power coefficient $= \sqrt[5]{\frac{\rho V^5}{P n^2}}$.

η, Efficiency.

n, Revolutions per second, r. p. s.

Φ, Effective helix angle $= \tan^{-1}\left(\frac{V}{2\pi r n}\right)$

5. NUMERICAL RELATIONS

1 hp. = 76.04 kg/m/s = 550 lb./ft./sec.
1 kg/m/s = 0.01315 hp.
1 mi./hr. = 0.44704 m/s
1 m/s = 2.23693 mi./hr.

1 lb. = 0.4535924277 kg.
1 kg = 2.2046224 lb.
1 mi. = 1609.35 m = 5280 ft.
1 m = 3.2808333 ft.